UNIVERSITY OF OKLAHOMA

GRADUATE COLLEGE

PARASEQUENCE-SCALE STRATIGRAPHIC VARIABILITY OF LITHOLOGY

AND POROSITY OF MISSISSIPPIAN MERAMEC RESERVOIRS AND THE

RELATIONSHIPS TO PRODUCTION CHARACTERISTICS, STACK TREND,

OKLAHOMA

A THESIS

SUBMITTED TO THE GRADUATE FACULTY

In partial fulfillment of the requirements for the

Degree of

MASTER OF SCIENCE

By

GARRETT HICKMAN
Norman, Oklahoma
2018

PARASEQUENCE-SCALE STRATIGRAPHIC VARIABILITY OF LITHOLOGY
AND POROSITY OF MISSISSIPPIAN MERAMEC RESERVOIRS AND THE
RELATIONSHIPS TO PRODUCTION CHARACTERISTICS, STACK TREND,
OKLAHOMA

A THESIS APPROVED FOR THE
CONOCOPHILLIPS SCHOOL OF GEOLOGY AND GEOPHYSICS

BY

Dr. Matthew J. Pranter, Chair

Dr. Andrew B. Cullen

Dr. John D. Pigott

This thesis is dedicated to my family. Their constant support and guidance throughout the

years has kept me pushing toward success. I would especially like to dedicate this thesis

to my late grandpa, Oakey Hagood.

ACKNOWELDGEMENTS

TABLE OF CONTENTS

LIST OF TABLES

LIST OF FIGURES

ABSTRACT

Mississippian Meramec reservoirs of the STACK (Sooner Trend in the Anadarko Basin of Canadian and Kingfisher counties) play in central Oklahoma consist of mixed siliciclastic and carbonate deposits. Depositional environments range from a clay-rich distal ramp margin setting to calcite-cemented lower shoreface and tidally influenced deposits. Meramec lithologies primarily consist of calcareous and argillaceous siltstones with some silty carbonates and silty mudstones that are defined based on the relative abundance of calcite cement, silica, and clay.

Combinations of gamma ray, density porosity, neutron porosity, bulk density, and deep resistivity logs were used with an Artificial Neural Network to classify lithologies in non-cored wells. Results show overall cross-validation accuracies of 88 – 91% in a training cored well and 73 – 83% in a testing cored well. User's accuracies for the lithologies vary significantly. Lithology logs and conventional well logs were used to establish a stratigraphic framework that is characterized by a hierarchy of nine shoaling-upward, northeast-southwest strike elongate parasequences that range from 80-150 ft (24-45 m) in thickness and are capped by marine-flooding surfaces. The lower four parasequences form four retrogradational sets that back-step to the northwest. Each of these sets is capped by a flooding surface. The lower Meramec is overlain by a succession of three cycles that form a aggradational to progradational succession. These are capped by two transgressive sequences at the top of the interval resulting in an overall relative sea level deepening in the Meramec.

Comparison of lithologies and mean petrophysical properties in horizontal wells show limited relationships with produced fluid volumes. Gas-oil-ratio (GOR) trends vary significantly across the study area. 30 to 180-day percent GOR changes suggest shallower, normally pressured reservoir conditions for wells in the structurally updip region of the study area. Wells producing from deeper reservoirs demonstrate potentially overpressured conditions. Reservoir pressure variability along with other factors such as fluid properties and completion techniques are likely significant controlling factors on production volumes, independent from wellbore lithology.

INTRODUCTION

Prior Studies

The Mississippian Meramec and the Devonian Woodford shale are the primary producing intervals of the STACK play (Sooner Trend in the Anadarko basin of Canadian and Kingfisher counties) in central Oklahoma. The Meramec reservoirs are, in part, the downdip equivalent of the historically prolific "Mississippi Lime" play in northern Oklahoma and southern Kansas. The "Mississippi Lime" is a broad term used to define all of the Mississippian-aged reservoirs of the Anadarko shelf in Oklahoma and primarily consists of carbonate and silica-rich deposits of Kinderhookian, Osagean, and Meramecian age (Parham and Northcutt, 1993). Extensive studies of the Mississippian limestone have identified multiple reservoir types based on depositional and diagenetic features that control reservoir properties (e.g., Watney et al., 2001, Grammer et al., 2013, Pranter et al., 2016). Numerous recent studies have investigated the depositional history and lateral variability of the Mississippian limestone in north-central Oklahoma (Mazzulo, 2011; LeBlanc, 2014; Birch, 2015; Lindzey, 2015; Turnini, 2015; Flinton, 2016; Mazzullo et al., 2016). Published studies of Meramec reservoirs in the STACK play are limited.

Mazzullo et al. (2016) compared well data in southern Kansas and northern Oklahoma to Kinderhookain and basal Meramecian outcrops in Missouri, Arkansas, and eastern Oklahoma to define a complex lithostratigraphic architecture of the strata. He found that subsurface Kinderhookian and lower Meramecian in Kansas and Oklahoma contained very similar lithofacies, depositional history, and stratigraphic architecture to

1

that observed in the outcrops of the tri-state area to the east. While the majority of his findings relate to the complexity of the underlying Kinderhookian and Osagean units to the north, he included analysis of a cored well in Garfield county, northern Oklahoma that contained the overlying undivided Meramecian and Chesterian units. From this core he determined that a single core would not serve as a type section for the interval. Rather, multiple wireline logs and sample descriptions were required to evaluate the complex nature of the Mississippian subsurface stratigraphy in the subsurface.

Price et al. (2017) used core data and wireline logs to show the Meramec is a dominantly siliciclastic system comprised of strike-elongate, northeast-southwest oriented, low-angle clinoforms interpreted to represent a subaqueous delta complex. He interprets the Meramec to be deposited during an overall rise in relative sea level. High-frequency relative sea-level changes are manifested in the form of stacked shallowing-upward parasequences that grade upward from argillaceous siltstones into calcareous siltstones (potential 4th-order cycles). Reservoir quality is interpreted to be influenced by the presence of clays that are believed to inhibit calcite cementation.

Data and Methods

This study constructs a sequence-stratigraphic framework for the Meramec in the STACK area and evaluates the spatial variability of lithology and porosity. The study area is located in parts of Blaine, Kingfisher, and Canadian counties in central Oklahoma. (Figure 1).

Figure 1. Map showing major tectonic provinces of Oklahoma. Study is shown by the black rectangle. (Modified from Campbell, et al., 1998; Dutton, 1984; Johnson and Luza, 2008; Northcutt and Campbell, 1995; LoCriccho, 2012; McConnell, 1989; Pranter et. al., 2016)

3

The following data have been used for this study: Two cored wells in east-central Blaine county, the Gulf Oil 1-23 Shaffer and Gulf Oil 1-25 Rohling. The Gulf Oil 1-23 Shaffer contains ~240 ft (74 m) of cored upper to middle Meramec and 23 thin-section photomicrographs with associated XRD data. The Gulf Oil 1-25 Rohling contains ~220 ft (67 m) of cored lower to middle Meramec and 30 thin-section photomicrographs with associated XRD data. Additionally, the Humble 1 Hawkins cored well with XRD and porosity data, but no well log data, was evaluated. The Hawkins well was used to validate the accuracy of porosity calculations. Data also include 175 wells with digital well-log data and 20 wells with production data. Well logs include: normalized gamma ray (GRNORM), deep resistivity (RESD), neutron porosity (NPHI), density porosity (DPHI), bulk density (RHOB), and caliper (CALI) logs. All wireline logs in the study area were provided by Warwick Energy.

An additional undisclosed cored well was provided by an operator to test the results of lithology classification models constructed from the Gulf Oil 1-25 Rohling and Gulf Oil 1-23 Shaffer cored wells.

GEOLOGIC SETTING

Structure

The Anadarko Basin is a northwest trending, asymmetrical foreland basin covering western Oklahoma and the Texas Panhandle (Beebe, 1959). The axis of the basin is adjacent and parallel to the Amarillo-Wichita uplift to the southwest (Adler, 1971), and at its deepest point, the basin contains greater than 40,000 ft (12,000 m) of

sedimentary section from Cambrian to Permian age (Ham et al., 1965; Gallardo and Blackwell, 1999). The basin is bounded by the Nemaha uplift to the east, the Arbuckle uplift to the southeast, the Amarillo-Wichita uplift to the west, the Hugoton embayment and Las Animas arch to the northwest, and the central Kansas Uplift to the north (Lane and De Keyser, 1980; Perry, 1990).

Paleotectonics

Formation of the Anadarko Basin can be divided into 3 major events: 1) Cambrian rifting of the Proterozoic continental crust 2) Cambrian to Early Mississippian thermal subsidence resulting in the formation of the southern Oklahoma trough, and 3) inversion of the intercontinental rift basin along basement-involved thrusts to produce a foreland basin during the late Paleozoic (Wickham, 1978, Perry, 1990, Keller and Stephenson, 2007). The Anadarko Basin has remained generally tectonically stable since the Permian (Ham et al., 1965).

Chronostratigraphy

Mississippian-age strata fall within the unconformity bounded transgressive - regressive cycle of the 2nd-order Kaskaskia sequence (Sloss, 1963; Manger, 2011). During this time ~350 ma., most of the craton was an extensive carbonate ramp. (Gutschick and Sandberg, 1983). Gutschick and Sandberg (1983) interpreted the outer

limit of the shelf edge to be at an average depth of 160 ft (50 m) with lateral variation along the margin due to underlying structure. The paleo-latitude of the study area was approximately 25° S in a humid to subtropical environment (Curtis and Champlin, 1959). During the Early Mississippian, a short regressive sea-level cycle resulted in shallow water, well-oxygenated environments (Frezon and Jordan, 1979). Significant relative sea-level fall occurred during the Late Mississippian and Early Pennsylvanian dominantly driven by the collision of the Laurentia and Gondwana continental plates. Post-lithification diagenesis and significant sub-aerial exposure resulted in multiple scales and types of mineral replacement and porosity development leading to a complex distribution of reservoir properties (Manger, 2011).

Lithostratigraphy

Mississippian strata are widespread across most of the Mid-Continent and are Kinderhookian, Osagean, Meramecian, and Chesterian in age. Previous studies have proposed specific nomenclature for formations within the Mississippian system in the Mid-Continent (Mazzullo, 2011) (Figure 2), but no formal nomenclature is currently accepted for the Meramecian sections in the study area. In the study area, the Kinderhookian strata consist of gray-green silty calcareous shales and silty dolomitic limestones. Osagean strata are primarily gray, finely crystalline, cherty limestone with variable abundance of chert, dolomite, and detrital silt with occurrences of brown calcareous shale (Curtis and Champlin, 1959; Rowland, 1961). The overlying
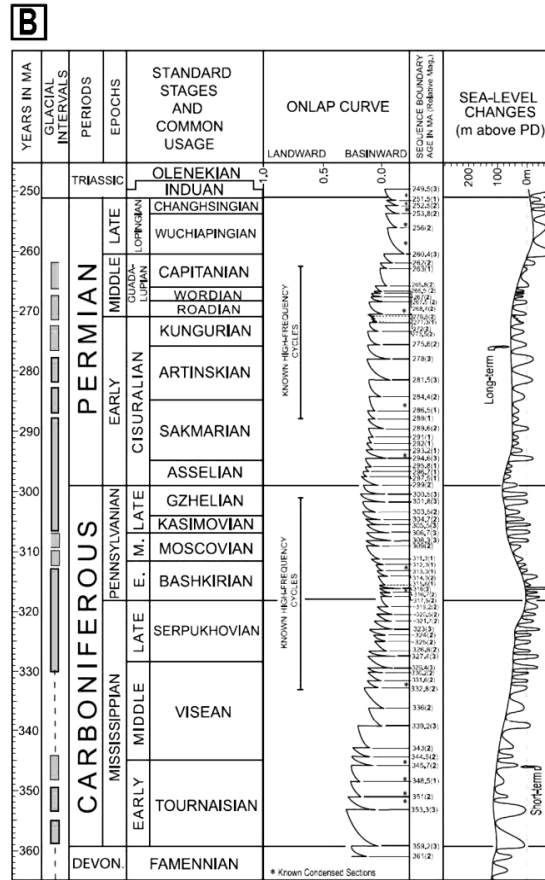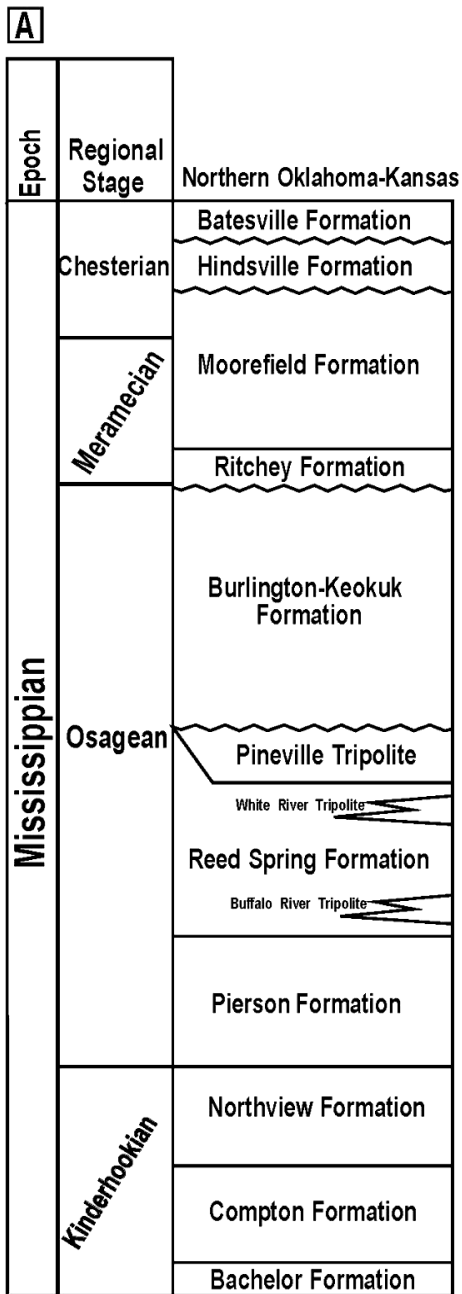
Figure 2. A) Idealized stratigraphic column of the Mississippian section (Modified from Mazzulo, 2011) The Meramecian interval is, in part, correlative to the Ritchey and Moorefield formations identified in Mazzullo (2011) B) Global sea level curve (Haq and Shutter, 2008). A global shift from greenhouse to icehouse conditions and global eustatic sea level fall indicate the relative sea level rise throughout the Meramec is controlled dominantly by continental collision and Pennsylvanian uplift.

Meramecian strata dominantly consist of gray calcareous and clay-rich calcareous

siltstones. Silty limestones and silty mudstone deposits are observed in lesser amounts.

The Chesterian units unconformably overly the Meramecian strata and are represented by

interbedded gray shale and limestone (Curtis and Champlin, 1959; Rowland, 1961).

METHODS

Core Descriptions of Lithology and Lithofacies

Two cored wells, the Gulf Oil 1-23 Shaffer and the Gulf Oil 1-25 Rohling (Figure

3 and Figure 4), in eastern Blaine county were described in terms of lithology, color,

grain size, bioturbation, and sedimentary structures to construct lithology and lithofacies

logs and interpret the depositional environments of the Meramec (Appendix B). The

lithofacies logs were constrained with XRD and thin-section photomicrographs. Core-log

depth corrections of +10 ft (3 m) for the Gulf Oil 1-25 Rohling and +5 ft (1.5 m) for the

Gulf Oil 1-23 Shaffer were made using a gamma ray scan log of the cored interval.

Lithofacies Classification

A supervised Artificial Neural Network (ANN) method was used to classify

lithofacies based on their open-hole log responses. Lithofacies logs and conventional well

logs were used to construct ANN relationships. Four combinations of normalized gamma

ray (GRNORM), deep resistivity (RESD), bulk density (RHOB), density porosity

(DPHI), and neutron porosity (NPHI) wireline logs were used to create ANNs for a

training well, the Gulf Oil 1-25 Rohling. The log combinations are as follows:
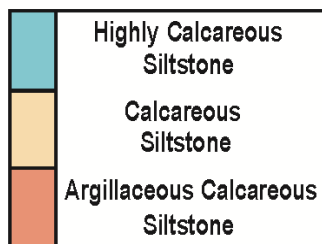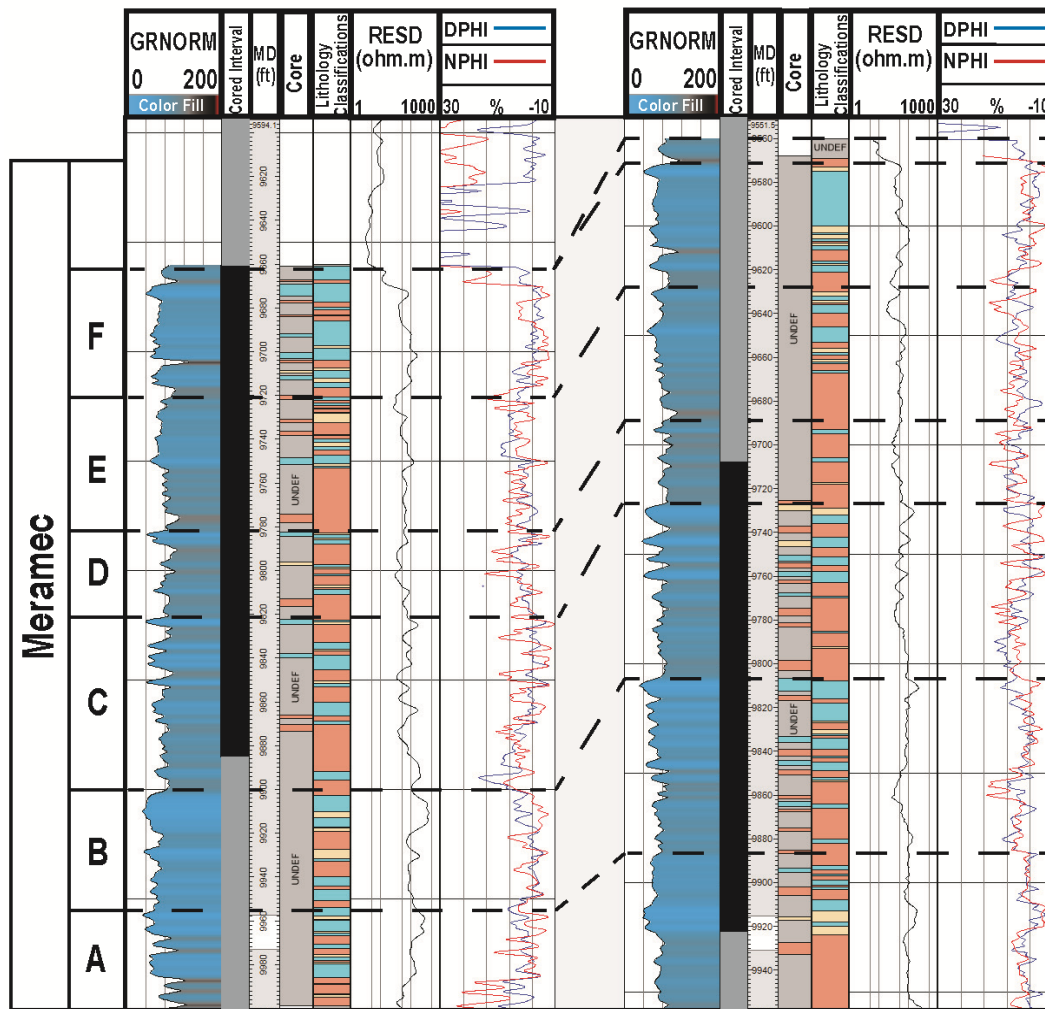
Figure 3. Gulf Oil 1-25 Rohling (training) and Gulf Oil 1-23 Shaffer (testing) cored wells used for lithology classification. Meramec parasequences present in core are shown. Cored intervals are shown as black highlighted interval. Core and classified lithology logs shown to the right of the depth track. Wireline logs presented were used for ANN training (GRNORM, NPHI, DPHI, RESD).
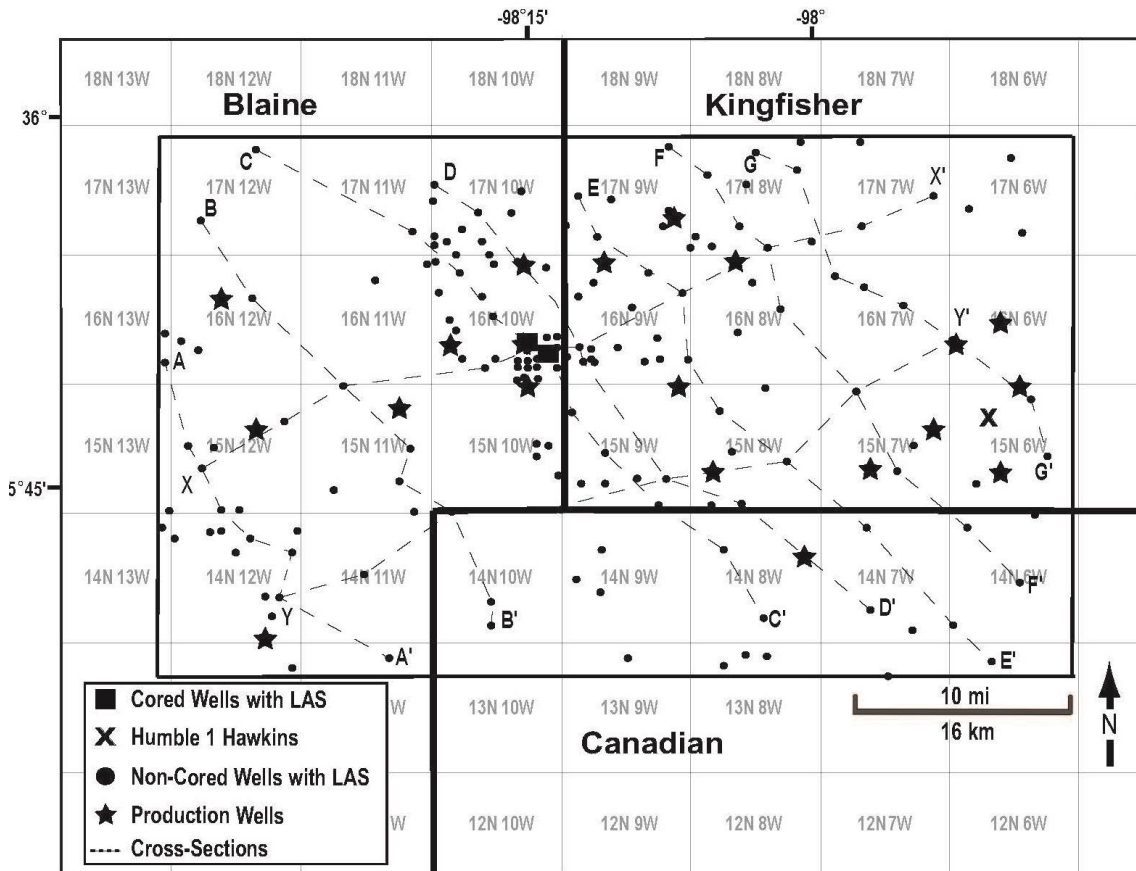
Figure 4. Study area basemap. Data include digital well logs from 175 wells, 2 cored wells (Gulf Oil 1-23 Shaffer and Gulf Oil 1-25 Rohling) with well logs, and one cored well with no well-log data (Humble 1 Hawkins). Dip-oriented cross-sections A-A' to G-G' and strike-oriented cross sections X-X' and Y-Y' were used to correlate Meramec parasequences. 20 wells with production data (stars) are

1. ANN 1: GRNORM, DPHI, RESD

2. ANN 2: GRNORM, DPHI, RHOB

3. ANN 3: GRNORM, NPHI, DPHI, and RESD

4. ANN 4: GRNORM, DPHI, and NPHI

An ANN is a classification method that compares input variables from well logs and iteratively weights each variable to optimize the accuracy of matching a target output (lithofacies logs). To internally determine the accuracy during the training process of the ANN, the data from the training well are split into two parts. 50% of the data in the training well is used to construct a relationship between the lithofacies log and wireline log curves. The other 50% is used evaluate the accuracy of the model by classifying lithofacies from the constructed relationships and comparing outputs with the target output. This process, known as cross-validation, is iterated until an optimum accuracy within a user-defined error threshold is achieved. Once the classification model was trained, each ANN suite was used to blind test classifications of the lithofacies in a testing cored well, the Gulf Oil 1-23 Shaffer. This process determines the accuracy of the classification model on a data set that is not biased to the training of the model.

An additional cored well with an undisclosed location approximately 7 mi (11 km) from the primary cored wells was used to classify lithofacies using the ANN to validate the results. Well-log data and a detailed core description were used for the process.

Accuracy of the classification models were determined using a confusion matrix. The accuracy for each class is determined by the number of correct classifications divided by the total data points for that class in the target output. The misclassification rate is equivalent to 1 (100%) minus the accuracy. Similarly, overall accuracy for all classes in the dataset is determined by dividing the total number of correct classifications by the total number of data points.

Stratigraphic and Structural Framework

The Meramec interval was divided into intervals (zones) based on well-log responses and the vertical succession of lithofacies. The zones were correlated for the 175 wells (Figure 4) using a combination of gamma ray, resistivity, and lithology logs. Zone tops were correlated across the study area using a grid of NW-SE and NE-SW trending cross-sections (Figure 4). Correlations from the grid of cross-sections were extended to all surrounding wells. Zone tops were identified based on an upward decreasing GRNORM signature associated with a high-magnitude negative GRNORM DTA value at top of each zone. Zones were also demarcated by subtle increases in the RESD log and anomalously high NPHI values as a response to clay-bound water. The zones exhibit higher-order cycles within them as defined by multiple finer scale cleaning-upward cycles. These higher frequency cycles were not correlated in this study. Structure-contour and isopach maps were constructed from the zone tops.

Derivative Trend Analysis

Identifying the parasequence-scale cycles in well logs was facilitated using a log-based approach called Derivative Trend Analysis (DTA) in Schlumberger's *Techlog*.

Using the GRNORM curves, DTA first smooths the log values over a user-defined interval using a Gaussian-smoothing function. The function assigns the log values a weight determined from its distance from the original point. The smoothed log is calculated by averaging the weighted values within a user-defined smoothing window height (Shapiro and Stockman, 2000; Wethington, 2017). Multiple smoothing windows were tested for this step ranging from 20 – 100 ft (6 – 30 m).

The second step of DTA calculates the derivative of the smoothed GRNORM curve between neighboring data points. DTA derivative curves are calculated using the central-difference formula as follows.

$$Derivative(i) = \frac{(Value(i+1) - Value(i-1))}{(Depth(i+1) - Depth(i-1))}$$

The derivative log displays positive and negative values dependent on the direction and magnitude of the slope of the smoothed curve. When the smoothed curve is decreasing upwards, the DTA curve calculates positive values with a magnitude dependent upon the rate at which the log is changing. Conversely, when the log is increasing upwards, the DTA curve calculates negative values (Figure 5) (Wethington, 2017).
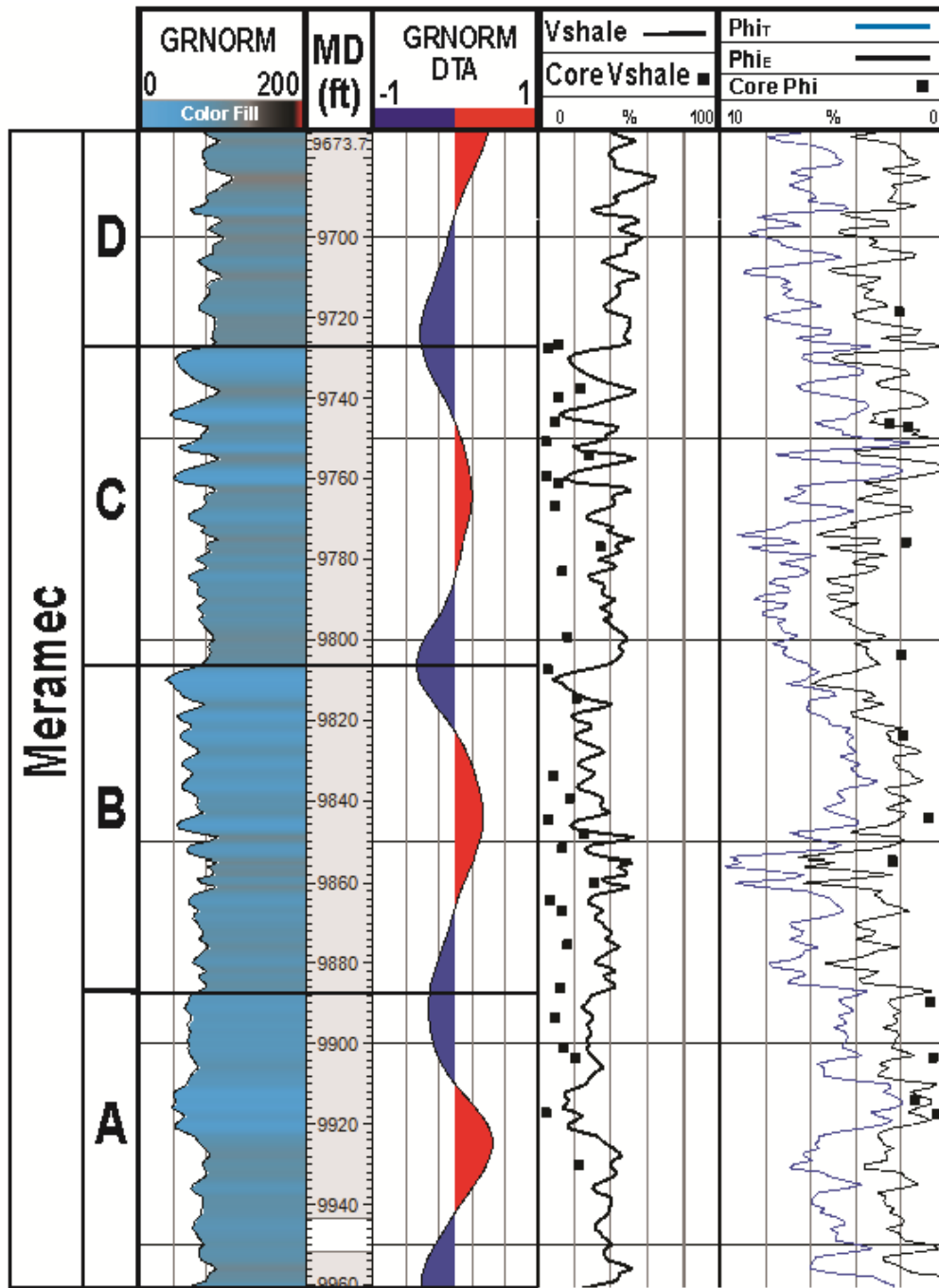
Figure 5. Gulf Oil 1-25 Rohling well-log section illustrating Derivative Trend Analysis (DTA) curve and parasequences. The flooding surfaces at the top of each parasequence correspond to high-magnitude, negative values in the DTA curve. Well-log-based calculations of V_{sh}, Φ_T, and Φ_E are shown to the right and compared to core measurements.

Meramec V_{sh}, Φ_T, and Φ_E

Log-based shale volume (V_{sh}), total porosity (Φ_T), and effective porosity (Φ_E)

logs were calculated for wells with GRNORM, DPHI, and NPHI wireline logs. Caliper

and RHOB logs were used to construct bad hole logs and identify invalid data to exclude

those intervals from the petrophysical calculations. Φ_T logs in the Meramec interval were

calculated using the root mean square (RMS) of NPHI and DPHI logs.

$$\Phi_T = \sqrt{\frac{DPHI^2 + NPHI^2}{2}}$$

To correct for clay-bound water, two empirical equations were used to calculate

V_{sh} and Φ_E logs. V_{sh} logs were calculated from the GRNORM log using the following:

$$V_{sh} = \frac{GRNORM_{log} - GRNORM_{min}}{GRNORM_{\max} - GRNORM_{min}}$$

Φ_E logs were calculated using the above V_{sh} calculations, Φ_T logs, and the average

porosity of the clay-rich zones (Φ_{AVGsh}). The following equation was used for calculation

of Φ_E logs:

$$\Phi_E = \Phi_T - (V_{sh} \times \Phi_{AVGsh})$$

V_{sh} and Φ_E calculations were compared to XRD data points and core derived porosity

values to determine the accuracy of these empirical calculations (Figure 5).

3-D Model Grid

Structure-contour maps for each zone were used to construct a stratigraphic

framework (3-D grid) covering ~1,050 mi^2 (~1,700 km^2). Aerial cell dimensions were

defined at 500 x 500 ft (150 x 150 m) with an average layer (cell) thickness of 2 ft (0.6 m) resulting in a 3-D grid with 32,128,284 cells. A proportional layering scheme was used for all zones except for the lower transgressive cycles (A-D). In these zones a "follow top" layering scheme with a defined cell thickness of 2 ft (0.6 m) was used to capture the onlapping character of the strata. For some zones in the model, the sequences did not extend across the study area due to onlap truncation. For these zones, surfaces were clipped where the isopach maps reached zero thickness to portray the truncating nature of cycles.

3-D Lithofacies Modeling

The lithology logs were upscaled to the model grid using an arithmetic averaging method and modeled using Truncated Gaussian Simulation (TGS) with trends and sequential Indicator simulation (SIS).

TGS with trends is a stochastic modeling technique constrained to upscaled well logs, variogram parameters, facies proportions by zone, expected vertical facies successions, and user-defined lateral facies trends. This method uses a traditional continuous Gaussian simulation algorithm in which cells within the model grid are randomly visited and assigned values. These values are assigned by analyzing neighboring cells and assigned values to honor distributions and variability defined by the primary inputs (lithofacies logs) and variogram parameters. TSG with trends is a useful in modeling situations in which a specific order of facies is observed. Vertical and lateral facies trends are defined and the cells are assigned values based on these trends in

16

conjunction with variogram parameters and lithofacies percentages. This results in a model that portrays the observed vertical lithofacies successions and variability and also honors the upscaled lithofacies logs (Pyrcz and Deutsch, 2014).

Placement of the boundaries between the lateral trends for each parasequence were interpreted from isopach maps constructed from the well tops (Figure 6). Another major input for the modeling process is the "variance" from the lateral trends defined. This is a measure of how much the trend for each lithofacies was weighted when interpreting between the wells. A higher variance value tends to more closely honor the upscaled lithofacies logs, with less emphasis on the defined trends. Conversely, a lower variance value produces results that emphasize the defined lithofacies trends. For the lithofacies models in this study, a high variance value of 1 was used to represent the significant lateral heterogeneity and vertical cyclicity within each parasequence.

SIS is a stochastic method that uses upscaled well-logs, vertical proportion curves, and variogram parameters to assign grid cell values. SIS is generally used to model highly variable or diagenetically controlled facies in which no noticeable vertical or lateral trends are observed. SIS assigns each grid cell a facies value by visiting each cell in a random order. Nearby and previously assigned cells are weighted using Kriging to determine the probable facies for the visited cell according to defined variogram parameters and facies distributions (Pyrcz and Deutsch, 2014). These assignments do not adhere to any defined vertical or lateral order of facies like TGS, so for reservoirs with discernable stacking patterns, facies successions observed in core and lithofacies logs are not represented in the resulting model between upscaled well log control.
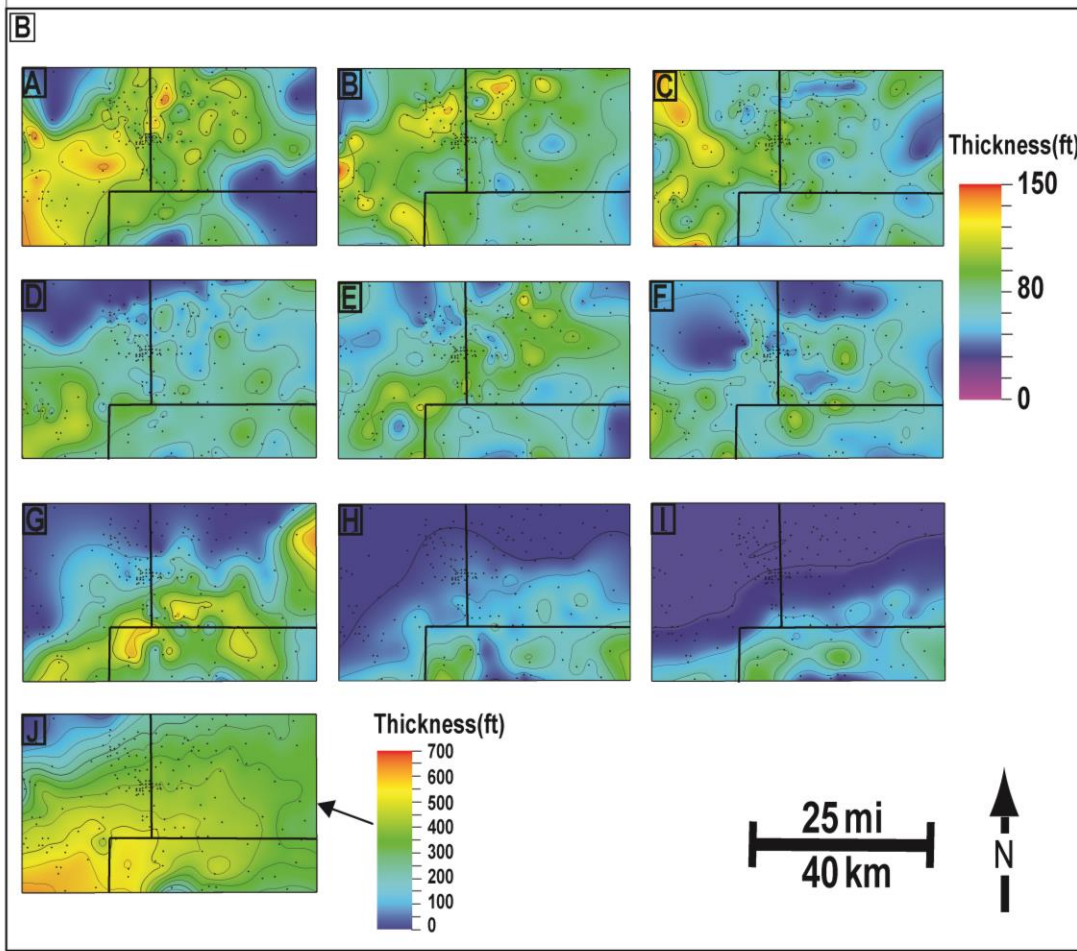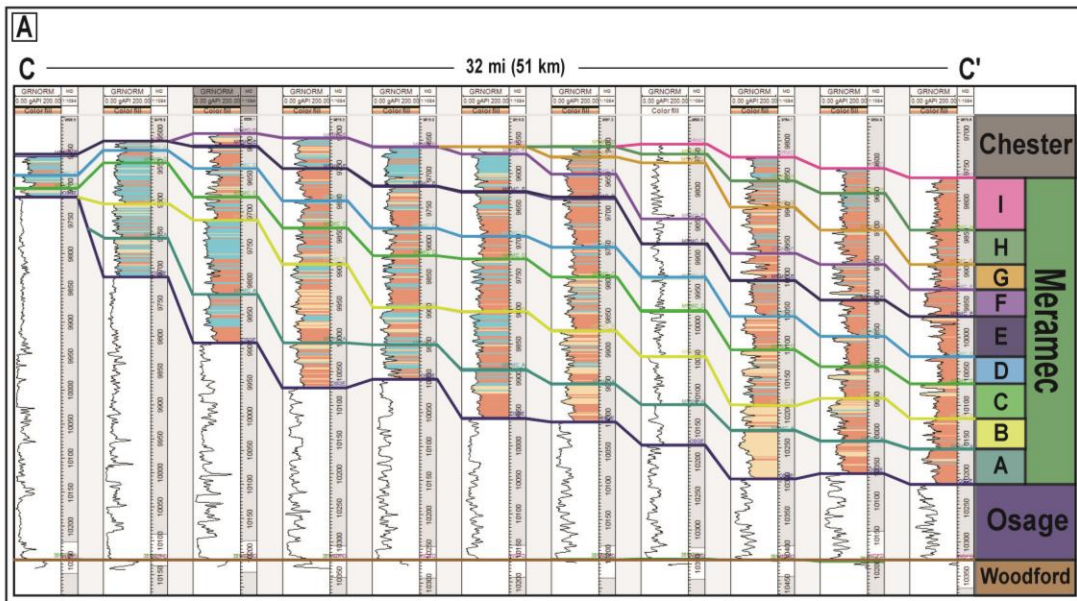
Figure 6. A) Representative dip-oriented cross section of Meramec parasequences. B) Parasequence isopach maps for sequences A-I. Isopach map of the entire Meramec interval is shown as J. Thickness trends indicate a depositional strike of approximately 60-75° from north with depositional dip to the southeast.

Petrophysical Modeling

Φ_T, V_{sh}, and Φ_E logs were upscaled to the 3-D grid using an arithmetic mean averaging method and biased to the lithofacies logs. Φ_T, V_{sh}, and Φ_E were modeled using sequential Gaussian simulation (SGS) and constrained to the 3-D lithofacies model. SGS is a stochastic modeling method similar to TGS and SIS in that each cell is randomly visited and assigned a value based on the values of the previously assigned surrounding cells, input variogram values, and a normal distribution of petrophysical values for that lithofacies. Azimuths in each zone for the major variogram direction matched azimuths used in the lithofacies modeling. Vertical variograms for Φ_T, V_{sh}, and Φ_E were determined independently for each zone and lithofacies using experimental variograms (Appendix F). From the models, mean maps of Φ_T, V_{sh}, and Φ_E models were calculated for the entire Meramec interval and each internal zone.

Relationship to Production Characteristics

The lithofacies and petrophysical property models were used to evaluate the relationships between production, lithology, and petrophysical properties using production data for 20 wells across the study area (Figure 4).

The productivity of each well was compared using 180-day barrel of oil equivalent (BOE) per foot of lateral surface volumes. BOE/ft values were calculated by dividing the 30 and 180-day BOE volumes produced by the length of the lateral wellbore for each well. To evaluate how geologic properties relate to well performance, petrophysical properties and lithofacies abundances were evaluated along the horizontal

well paths for each well. However, the necessary NPHI, DPHI, and RESD well-log data do not exist for the horizontal well paths to directly classify lithofacies using the ANNs or to calculate petrophysical properties from wireline logs. Therefore, synthetic horizontal well logs were constructed from the lithofacies and petrophysical property models by extracting data along the well bore where it intersects the model cells. Mean values for petrophysical properties and lithofacies percentages determined by the synthetic logs were calculated and related to the performance of each well.

To evaluate the variations in produced surface fluid properties, gas-oil-ratio GOR values were calculated for 30-day and 180-day total production volumes for each well. The values were mapped on a structure map of the Meramec to determine the control of reservoir depth on 30-day and 180-day GOR. The % change of GOR from 30 to 180 day total volumes was also calculated as a proxy for variability in reservoir pressure across the study area.

RESULTS

Lithology and Lithofacies Classification

In the cored Meramecian intervals described in the Gulf Oil 1-25 Rohling and Gulf Oil 1-23 Shaffer, 6 dominant lithofacies were identified based on observations of lithology, color, sedimentary structures, and diagenetic textures. The lithofacies are 1) calcareous siltstones, 2) bioturbated calcareous siltstones, 3) laminated argillaceous calcareous siltstones, 4) bioturbated argillaceous calcareous siltstones, 5) silty skeletal pack-grainstones and 6) silty mudstones. (Figures 7 and 8) (Table 1)
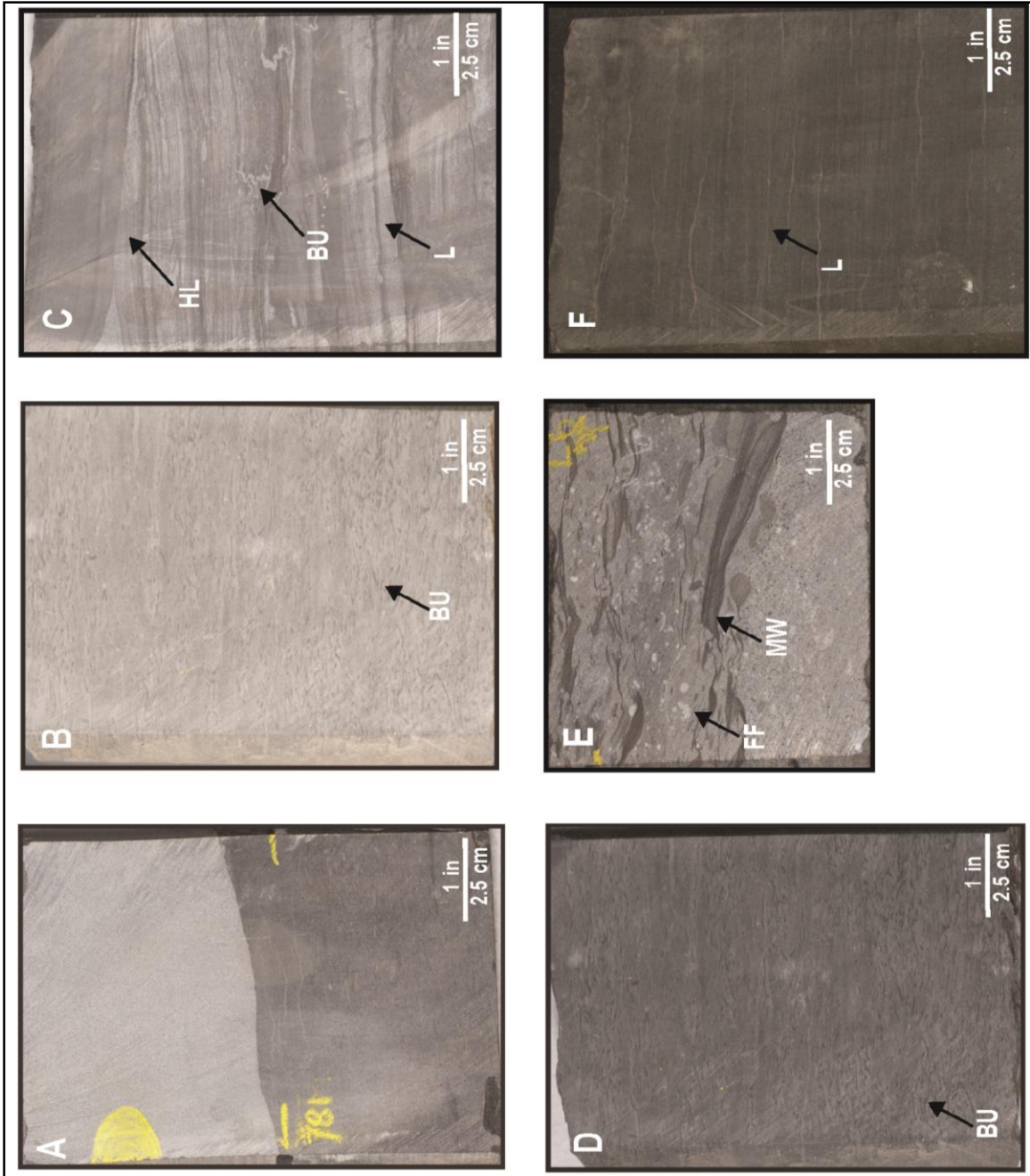
Figure 7. Photographs of Meramec lithofacies identified in core: A) calcareous siltstone (Gulf Oil 1-23 Shaffer 9831 ft [2996 m] MD). B) Bioturbated calcareous siltstone (Gulf Oil Rohling 1-25 9894 ft [3015 m] MD). C) Laminated argillaceous calcareous siltstone (Gulf Oil 1-23 Shaffer (9679 ft [2950 m] MD). D) Bioturbated argillaceous calcareous siltstone (Gulf Oil 1-25 Rohling 9661 ft [2944 m] MD). E) Silty fossiliferous pack-grainstone (Gulf Oil 1-23 Shaffer 9697 ft [2955 m] MD). F) Silty Mudstone (Gulf Oil 1-23 Shaffer 9663 ft [2945 m] MD). Legend: BU=bioturbation; L=lamination; HL=hummocky lamination; FF=fossil fragments; MW=mudstone whisps.
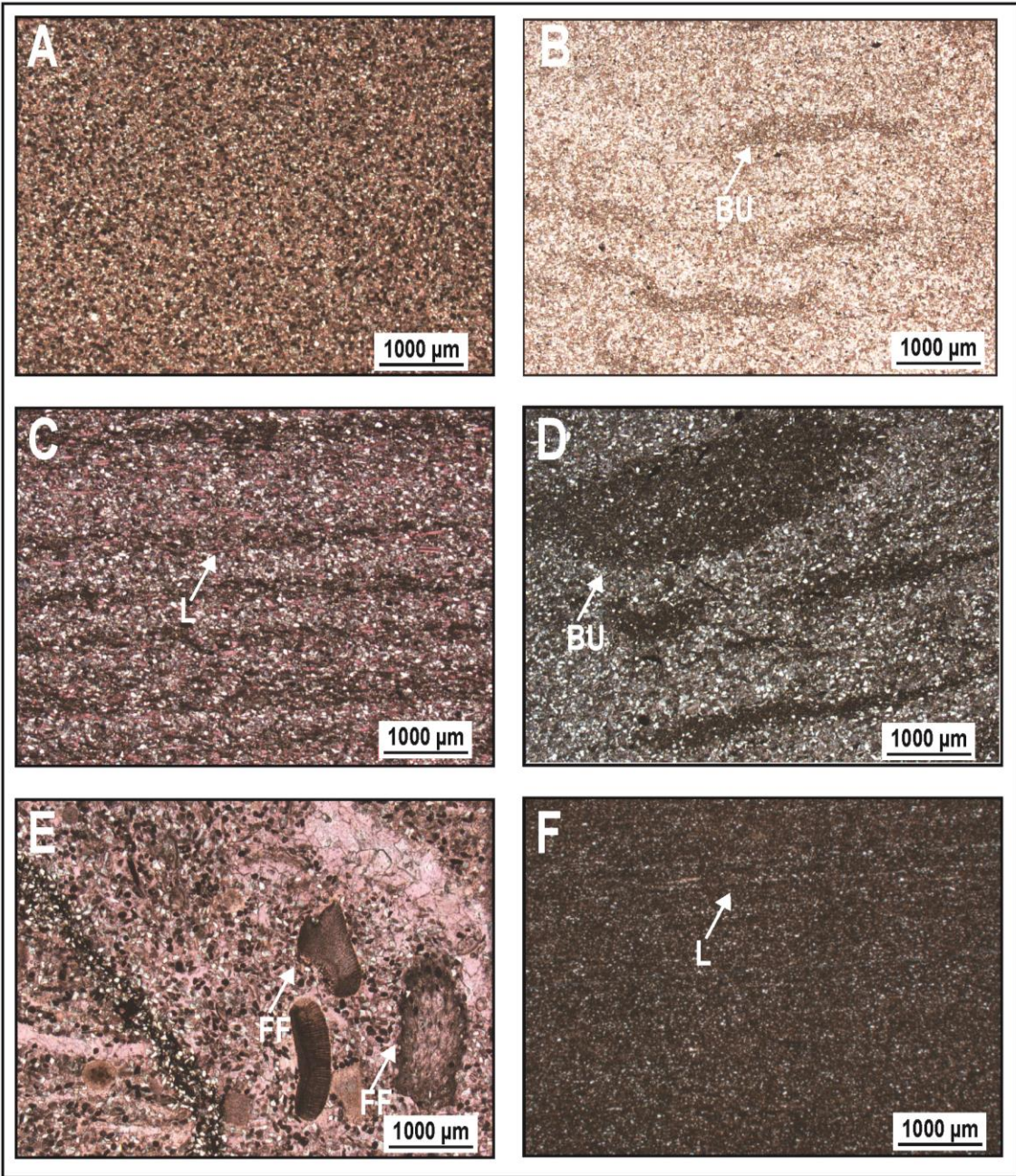
Figure 8. Thin section photomicrographs of Meramec lithofacies. A) Calcareous siltstone. Silt-sized, well-sorted, sub-rounded to sub-angular quartz grains with intergranular calcite and some peloids and horizontal to wavy laminations (Gulf Oil 1-23 Shaffer 9832 ft [2997 m] MD). B) Bioturbated calcareous siltstone. Silt-sized, sub-rounded to sub-angular, quartz grains with calcite cement and low bioturbation. Burrows are clay-filled (Gulf Oil 1-25 Rohling 9920 ft [3023 m] MD). C) Laminated argillaceous calcareous siltstone. Silt-sized, sub-rounded to sub-angular quartz grains with lesser amounts of calcite and elevated levels of intergranular and laminated clay material. Horizontal to wavy laminations with some hummocky cross-stratification (Gulf Oil 1-23 Shaffer 9678 ft [2950 m] MD). D) Bioturbated argillaceous calcareous siltstone. Heavily bioturbated with silt-sized, sub-rounded to sub-angular quartz grains. Decreased calcite content with prominent intergranular clay minerals (Gulf Oil 1-25 Rohling 9891 ft [3014 m] MD). E) Silty fossiliferous pack-grainstone. Abundant calcite and fossil fragments with some peloids and silt-sized, sub-angular quartz grains (Gulf Oil 1-23 Shaffer 9663.2 ft [2945.2 m] MD). F) Silty mudstone. Faintly laminated, clay-rich with some calcite and decreased abundance of silt-sized quartz grains (Gulf Oil 1-23 Shaffer 9676 ft [2949 m] MD). Legend: BU=bioturbation; L=lamination; HL=hummocky lamination; FF=fossil fragments; MW=mudstone whisps.

Lithofacies	Description	Depositional Environment
Calcareous Siltstone	Silt-sized quartz grains with varying amounts of calcite cement up to 70%. Occasional peloids and fossil fragments with occurrences of parallel and wavy laminations with some hummocky cross - stratification.	Inner ramp - within or around fair-weather wave base.
Bioturbated Calcareous Siltstone	Dominantly silt-sized quartz grains with varying amounts of calcite up to 40%. Peloids and light bioturbation vary throughout.	Inner ramp - below fair-weather wave base.
Laminated Argillaceous Calcareous Siltstone	Silt-sized quartz grains with some calcite cement and varying amounts of laminated and intergranular clay. Occasional peloids and fossil fragments.	Mid-outer ramp - at or near storm wave base.
Bioturbated Argillaceous Calcareous Siltstone	Silt-sized quartz grains with some calcite cement, intergranular clay, and abundant, dark, clay-filled burrows. Some fossil fragments.	Outer ramp to ramp crest - below storm wave base.
Silty Skeletal Pack-Grainstone	Abundant fossil fragments, peloids, and calcite cement with some intergranluar silt-sized quartz grains. Little to no clay minerals.	Lower shoreface to inner ramp - Above fair-weather wave base.
Silty Mudstone	Dominantly clay minerals with some detrital silt-sized quartz grains and calcite cement. Minor shell fragments and faint horizontal laminations.	Distal ramp edge near basin environment. Well below storm wave base.

Table 1. Descriptions of Meramecian lithofacies identified in core. Key components and sedimentary structures are included with interpreted depositional environments.

Initial ANN testing runs found that many of the small-scale differences in the lithofacies such as sedimentary structures were not manifested in well log responses. This lack of differentiation did not allow individual lithofacies to be classified accurately using the ANN models. Therefore, lithology logs were constructed in the cored wells based on parent lithologies of the lithofacies. These lithologies are:

1) Calcareous siltstones: intervals of dominantly silica minerals (>50%), greater than 15% calcite, and less than 15% clay. Silica grains are primarily well-sorted, sub-rounded, silt-sized quartz grains with some potassium and plagioclase feldspars.

2) Argillaceous calcareous siltstones: contain greater than 20% clay minerals with varying abundances of silica and 10 – 20% calcite.

3) Highly calcareous siltstones: contain over 50% calcite and varying abundances of silica with minimal amounts of clay.

 Silty skeletal packstones and grainstones are also present but represent a very small percentage of the observed lithofacies and could not be differentiated in well-log response from the highly calcareous siltstones. Therefore, no unique lithology was defined for this lithofacies and they are included in the highly calcareous siltstone parent lithology.

In the Gulf Oil 1-25 Rohling training well, cross-validation classification accuracies ranged from 88 – 91%. The different ANN well-log suites produced very similar overall accuracies, yet showed a range in the user's accuracies of the individual lithologies from 48 – 98% (Appendix C).

After the ANN training process, lithologies were classified in the Gulf Oil 1-23 Shaffer well and compared with the lithology log from core. Overall accuracies for the testing well for the different log suites range from 48 – 80%. User's accuracies of the individual lithologies for the different well log suites varied from 0-93% (Appendix C). ANN 3 was selected as the best overall classification model for classifications in the non-cored wells due to having a high overall accuracy (80%) and the most optimistic user's accuracies (53-93%) out of the different well log suites. This log suite was used for subsequent modeling of lithology across the study area. Calcareous siltstone and highly calcareous siltstone lithologies are the most commonly misclassified lithologies. In the blind test on the Gulf Oil 1-23 Shaffer classified using ANN 3, 41% of calcareous siltstones identified in core were classified as highly calcareous siltstones, and 18% of highly calcareous siltstones were classified as calcareous siltstones (Table 2) (Appendix C). This is likely a result of the subtle log response differences between these two lithologies. The user's accuracy using ANN 3 for the argillaceous calcareous siltstone lithology was 93%. The classified lithology logs compared to core lithologies in the training and testing wells is shown as Figure 3.

When lithologies were classified in the non-cored wells, it was observed that some intervals southeast of the cores with high GRNORM values indicative of abundant clay minerals were estimated as highly calcareous siltstone. This was assumed to be anomalous and in the final model, a GRNORM threshold of 100 API units was set for the argillaceous calcareous siltstone. Intervals exhibiting values over this threshold were manually set to argillaceous calcareous siltstone. Additionally, wells to the southeast in

A	**Actual Lithologies**		
ANN 3 Predicted Lithologies 80% Accuracy	**Calcareous Siltstone (1)**	**Argillaceous Calcareous Siltstone (2)**	**Highly Calcareous Siltstone (3)**
1	9	3	15
2	1	72	3
3	7	8	68
User's Accuracies	53%	93%	90%

B	**Actual Lithologies**		
ANN 3 Predicted Lithologies 55% Accuracy	**Calcareous Siltstone (1)**	**Argillaceous Calcareous Siltstone (2)**	**Highly Calcareous Siltstone (3)**
1	28	37	59
2	57	311	52
3	95	87	77
User's Accuracies	16%	71%	53%

Table 2. Confusion matrix illustrating classification accuracy for the cored wells using the ANN 3 log suite (GRNORM, NPHI, DPHI, RESD). A) Blind test classification accuracy for the Gulf Oil 1-23 Shaffer testing well. B) Blind test classification accuracy for the undisclosed cored well.

the study area exhibited intervals with GRNORM values >170 API units. These intervals were determined to likely represent rocks with increased organic content not represented in core and similar to those identified by Miller (2018). Since these lithologies were not included in the ANN training, they were manually defined as a separate organic mudstone lithology.

Classifications of lithologies in the undisclosed cored well yielded less accurate results (55% overall accuracy). Individual user's accuracies for the lithologies varied significant with 16% in the calcareous siltstone, 71% in the argillaceous calcareous siltstone, and 53% in the highly calcareous siltstone (Table 2).

Stratigraphic and Structural Framework

The Meramec ranges in thickness from 50 ft (80 m) – 600 ft (970 m) with the thickest interval in the southwest of the study area near the deeper parts of the Anadarko Basin and thins toward the north on the Anadarko shelf (Figure 6 and 10). Nine shallowing upward cycles (A-I) were identified based on core lithologies and well log responses. These cycles are generally represented as argillaceous calcareous siltstones, calcareous siltstones, and highly calcareous siltstone lithologies from base to top. Stacking patterns are identified by a decreasing upward GRNORM motif capped by a sharp increase indicating a flooding surface. Often the observed cycles from core and logs exhibit multiple levels of cyclicity within a zone (e.g., 3rd order) (Price et al., 2017; Figure 9).
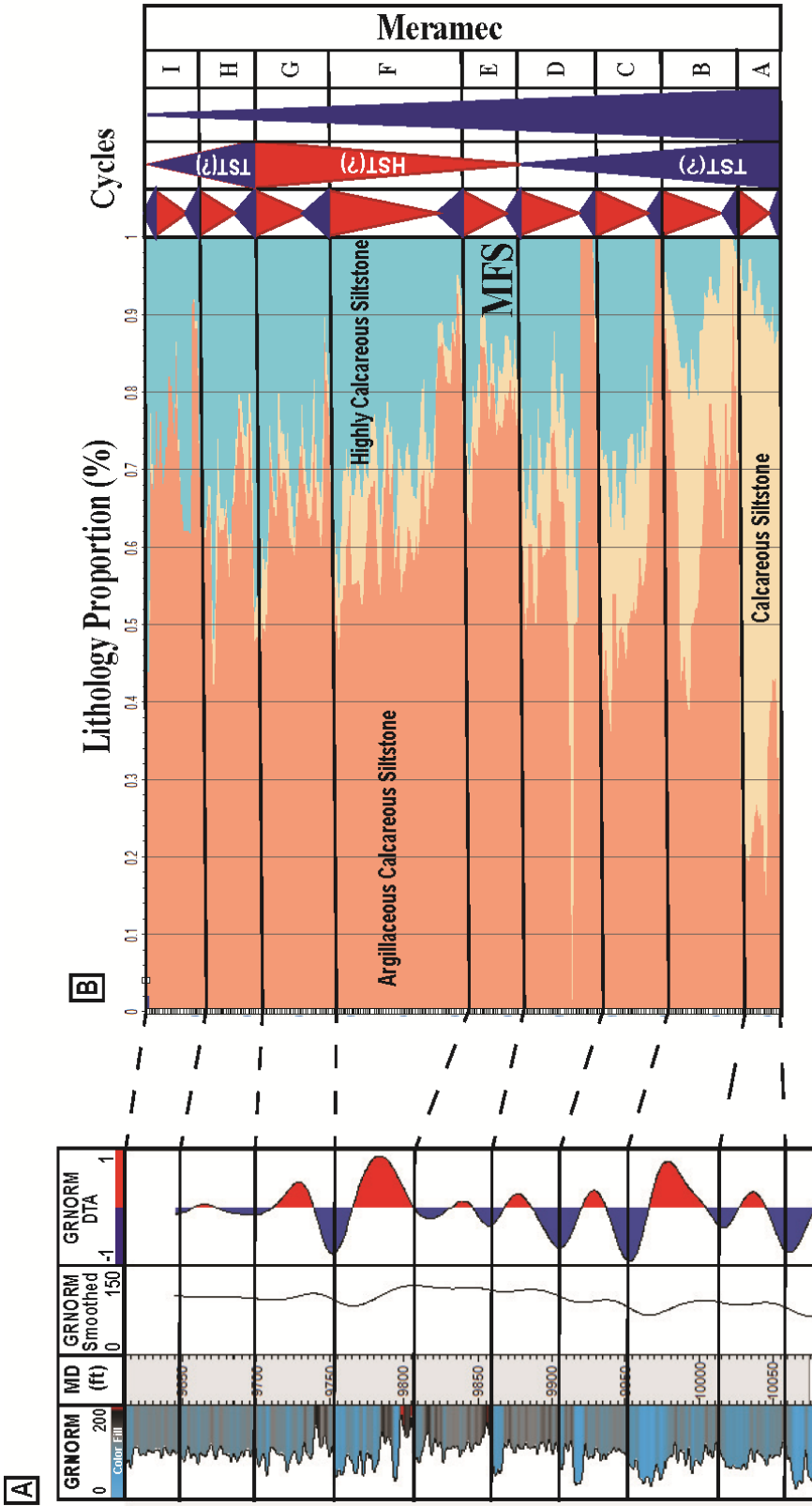
Figure 9. A) Log track displaying GRNORM, smoothed GRNORM, and GRNORM DTA log curves with interpreted sequence tops. B) Meramec vertical lithology proportion curve. The Meramec is interpreted to have been deposited during a lower order transgressive cycle. Parasequences A-D represents a retrogradational parasequence set that is capped by the maximum flooding surface. Parasequences E-G represent a progradational parasequence set. Parasequences H and I are interpreted to represent a final transgression resulting in an overall deepening of relative sea level during the Meramecian (Price et al., 2017)
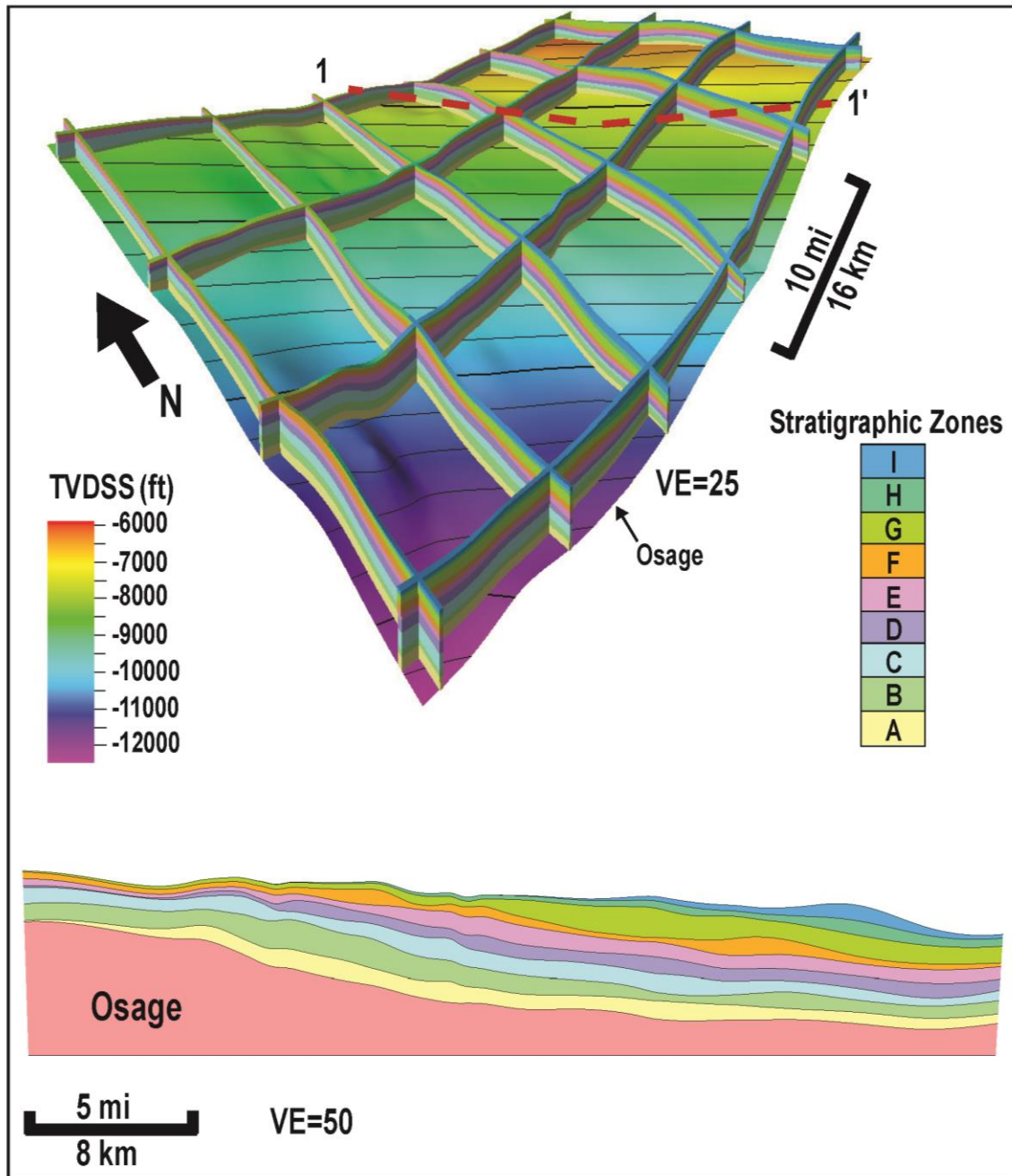
Figure 10. Meramec sequence-stratigraphic framework model. Cross-section C-C' shows the retrogradational and progradational parasequence sets. Underlying Osage structure-contour map displayed for reference. Cross sectional view is flattened on the Woodford shale.

Flooding surfaces bounding cycles at the scale of interest were easily identified using the GRNORM DTA calculated logs from the derivative trend analysis (Figure 5). A 35 ft (10 m) window was determined to produce the optimal resolution of flooding surfaces capping the parasequences.

The flooding surfaces capping each zone were characterized by a high magnitude, negative DTA value relating to the increase in GRNORM log motifs. Each zone is variable in thickness across the study area from 0 ft (0 m) to 150 ft (45 m) and contains a strike elongate, northeast-southwest trending thickness (Figure 6). Dip oriented thickness trends in the lower Meramec (A-C) were observed and are interpreted to potentially represent turbidite flows suggested by Price et al. (2017) and Miller (2018).

The lower four Meramec zones (A, B, C, D) are interpreted to form four retrogradational parasequence sets composed of shoaling upward cycles. Argillaceous calcareous siltstone lithology percentage in each parasequence gradually increases upwards from zone A to zone D (Figure 9). Parasequences E, F, and G represent a basinward shift in deposition and form a progradational parasequence set. Calcareous siltstone and highly calcareous siltstone lithologies become more abundant and flooding surfaces are increasingly less pronounced from the GRNORM log signatures. The boundary between sequences A-D and E-G is interpreted to represent a maximum flooding surface for the Meramec interval (Figure 9). Based on GRNORM log profiles, the top two Meramec parasequences (H and I) exhibit an increase in clay content and are interpreted to represent a final set of retrogradational parasequences that are capped by a flooding surface at the top of the Meramec interval (Figure 6 and Figure 9). This

transgression is believed to result in an overall deepening of the Meramec that leads into the deposition of the overlying deep-water Chesterian shales and limestones. Similar sequence-stratigraphic interpretations of the Meramec interval in the STACK area have been proposed by Price et al. (2017) (Appendix E) and Miller (2018).

Meramec V_{sh}, Φ_T, and Φ_E

Meramec V_{sh}, Φ_T, and Φ_E calculations were made in wells with GRNORM, DPHI, and NPHI logs. The V_{sh}, Φ_T, and Φ_E log values were compared to core-derived measurements from the Gulf Oil 1-23 Shaffer and Gulf Oil 1-25 Rohling (Figure 5).

For the calculation of V_{sh} logs, GRNORM$_{min}$ and GRNORM$_{max}$ values were determined to be 20 and 170 API units respectively from visual analysis of the "cleanest" and "hottest" GRNORM values observed within the Meramec interval. Some intervals in the southeast of the study area exhibited GRNORM values >170 API units and up to 220 API. These intervals were interpreted to represent an organic mudstone facies not represented in core, and were not used in calculations of V_{sh} or Φ_E logs.

Calculated Φ_T logs exhibited porosities ranging from 0 – 35%, which is much greater than the range for core porosities (0-6%) (Figure 5). These high porosity calculations can likely be attributed to the effect that clay-bound water has on NPHI logs.

Although V_{sh} logs tend to overestimate values derived from XRD, they capture the vertical trends of clay content in the sequences. V_{sh} values range from 0 – 100%, with a mean of 2%. For calculations of the Φ_E logs, Φ_{AVGsh} values in sequences A-G were interpreted from cross plots of Φ_T and V_{sh} to be 8%. Φ_{AVGsh} values for the upper two

Meramec parasequences (H & I) were found to be higher than the underlying A-G parasequences at 15% and 12% respectively. Therefore, three separate Φ_E logs were calculated for the varying Φ_{AVGsh} intervals and combined into a single Φ_E log. Resulting Φ_E logs exhibit a high correlation to core porosities. Φ_E values range from 0-10% with a mean of 2.5%. The higher Φ_E values are mostly observed in the distal portions of the area where V_{sh} calculations are higher.

Porosity values over 5% are not observed in the core data from the Gulf Oil 1-25 Rohling or the Gulf Oil 1-23 Shaffer. However, the Humble 1 Hawkins well (Figure 4) in south-central Kingfisher county has core-measured porosities up to 9.5% (Appendix D). Log data are not available for the Hawkins to correlate log-based calculations to core-measured values.

Price et al. (2017) suggested that clay-rich facies with lower depositional porosity were less prone to calcite cementation, thereby preserving interparticle pore space. This is a possible explanation for the Φ_E to V_{sh} relationship interpreted from these data. Additionally, Shelly et al. (2017) and Cullen (2017) observed a strong relationship between porosity and permeability in the Meramec interval. Shelly et al. (2017) studied a rock quarry in northeastern Oklahoma as an analog for subsurface Meramec strata in the mid-continent. He observed that permeability from core plugs of the facies in outcrop to be directly correlated to average porosity. Permeability measurements from the core plugs were low, ranging from 0-0.0025 mD (Appendix D). A similar relationship between porosity and permeability is observed in the same cored wells used in this study (Gulf Oil 1-23 Shaffer and Gulf Oil 1-25 Rohling) by Cullen (2017). Permeability values

up to 0.01 mD are associated with porosities up to 4%. These calcite-porosity and porosity-permeability relationships lead to the observation that the argillaceous lithologies are likely to exhibit the highest reservoir quality.

Lithology Models

Horizontal variogram parameters for both SIS and TGS with Trends models were set at 5,000 ft (1500 m) in the major direction and 3,500 ft (1,050 m) in the minor direction with major direction azimuths varying from 60-75 degrees from north. Azimuths for each zone were determined from isopach thickness maps of the sequences (Figure 6). Vertical variogram values were determined for each model zone from experimental variograms and range from 9 to 16 ft (2.7 to 5m) (Appendix F).

The resulting SIS model exhibited a highly varied distribution of lithologies across the study area and did not replicate vertical facies successions observed in core and lithology logs or the idealized lateral depositional model for the system (Figure 11). This was particularly evident in areas of the model with sparse data. The large well spacing imposed larger interpolation distances in these sections of the models. The large interpolation distances, short horizontal variogram parameters, and lack of user defined lithology trends resulted in lithologies being assigned to grid cells that do not conform to the idealized depositional model. For example, increased amounts of highly calcareous siltstones were present in the southeast distal portion of the study area where more argillaceous deposits were expected. Conversely, larger amounts of argillaceous lithologies were populated in cells to the northeast in the proximal environments.

36
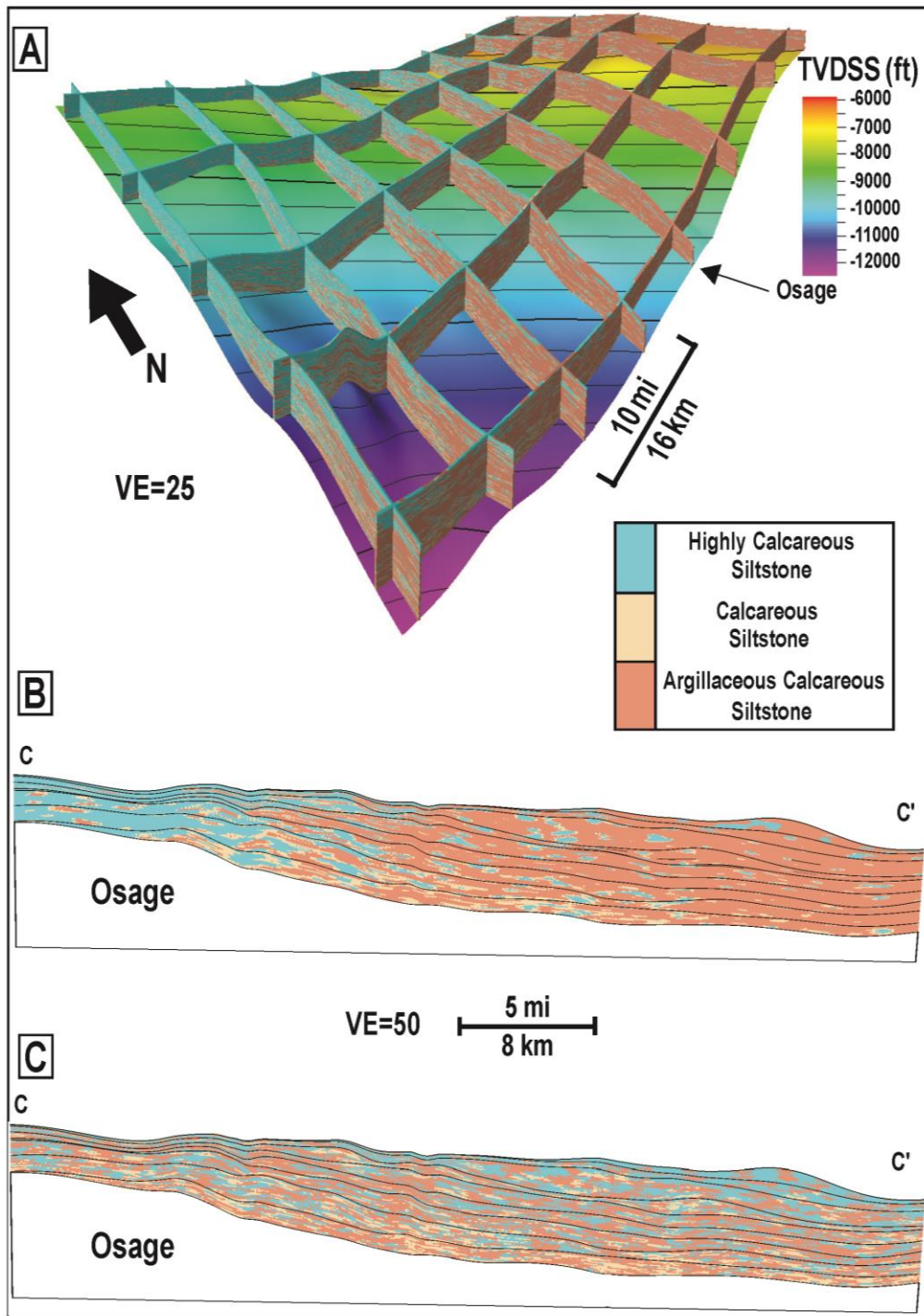
Figure 11. A) Lithology model fence diagram. Osage structure-contour map displayed for reference. B) Cross section C-C' illustrates the lithology distribution using B) TGS and C) SIS. Increasing clay content observed toward the southeast. Cross sectional views are flattened on the Woodford

37

The lithology model constructed using TGS with trends closely represents the retrogradational to progradational facies distribution for the Meramec interpreted from the vertical proportion curve (Figure 9 and 11). In the lower Meramec, the boundary between the lower-depositional energy argillaceous calcareous siltstones and higher energy calcareous siltstone lithologies can be seen migrating northwest from through the A to D parasequences, owing to relative sea level transgression. As a result, the D and E parasequences exhibit the highest overall abundance of argillaceous lithologies and lesser amounts of calcareous and highly calcareous siltstones (Figure 9). Sequences E-G contain a decreasing amount of argillaceous lithologies from base to top a result of progradation to the southeast. Calcareous siltstone lithologies are also less prominent than in the lower A-D zones. This is interpreted to be a result of falling sea-level promoting increased calcite cementation in the shallower depositional environments.

Meramec V_{sh}, Φ_T, and Φ_E Models

Horizontal variogram values for the petrophysical models were set at 2,500 ft (762 m) in the major direction and 1,700 ft (518 m) in the minor direction. These values were set to be less than the horizontal variograms of the lithology models to capture the variations of petrophysical properties within each lithology. Vertical variograms were determined from experimental variograms and vary by zone and lithology (Appendix F). When constraining petrophysical properties to individual lithologies, some anomalous values were observed in the highly calcareous lithologies. V_{sh} values over 15% and Φ_E values over 6% were observed. This was interpreted to likely be attributed to

38

petrophysical values of argillaceous zones being associated with intervals misclassified as highly calcareous siltstones in the predicted lithology logs. These values were truncated and excluded from the model to constrain petrophysical values to those observed in core. Models of V_{sh} and Φ_E generally exhibit greater values to the to the southeast (Figures 12, 13, and 14; Appendix F). The increasing porosity to the southeast is positively correlated to a greater percentage of argillaceous lithologies in the lithology model. Similarly, higher Φ_E are observed in the zones that contain a greater amount of argillaceous calcareous siltstone. In zones A-D, both V_{sh} and Φ_E are observed to increase upward as the transgressive sequences backstep to the northwest, resulting in more argillaceous deposits in the C and D sequence sets. As the system begins to prograde back towards the basin, both properties in the E-G sequences decrease upward as a result of an increasing abundance of calcareous and highly calcareous lithologies (Figure 9 and 12). Both the H and I parasequences exhibit high V_{sh} and Φ_E due to the subsequent transgression of the system. However, the Φ_T model exhibits anomalously high values relative to the underlying section and no core data was available for these sequences to validate calculated petrophysical values in these zones. This lack of core data causes uncertainty to the validity of these calculations. For the purpose of evaluating reservoir potential, the D and E parasequence sets bounded by the maximum flooding surface exhibit the highest average V_{sh} and Φ_E. V_{sh} average values are approximately 50% and 45%, and Φ_E average values are approximately 4% and 5% respectively (Figure 13 and 14).
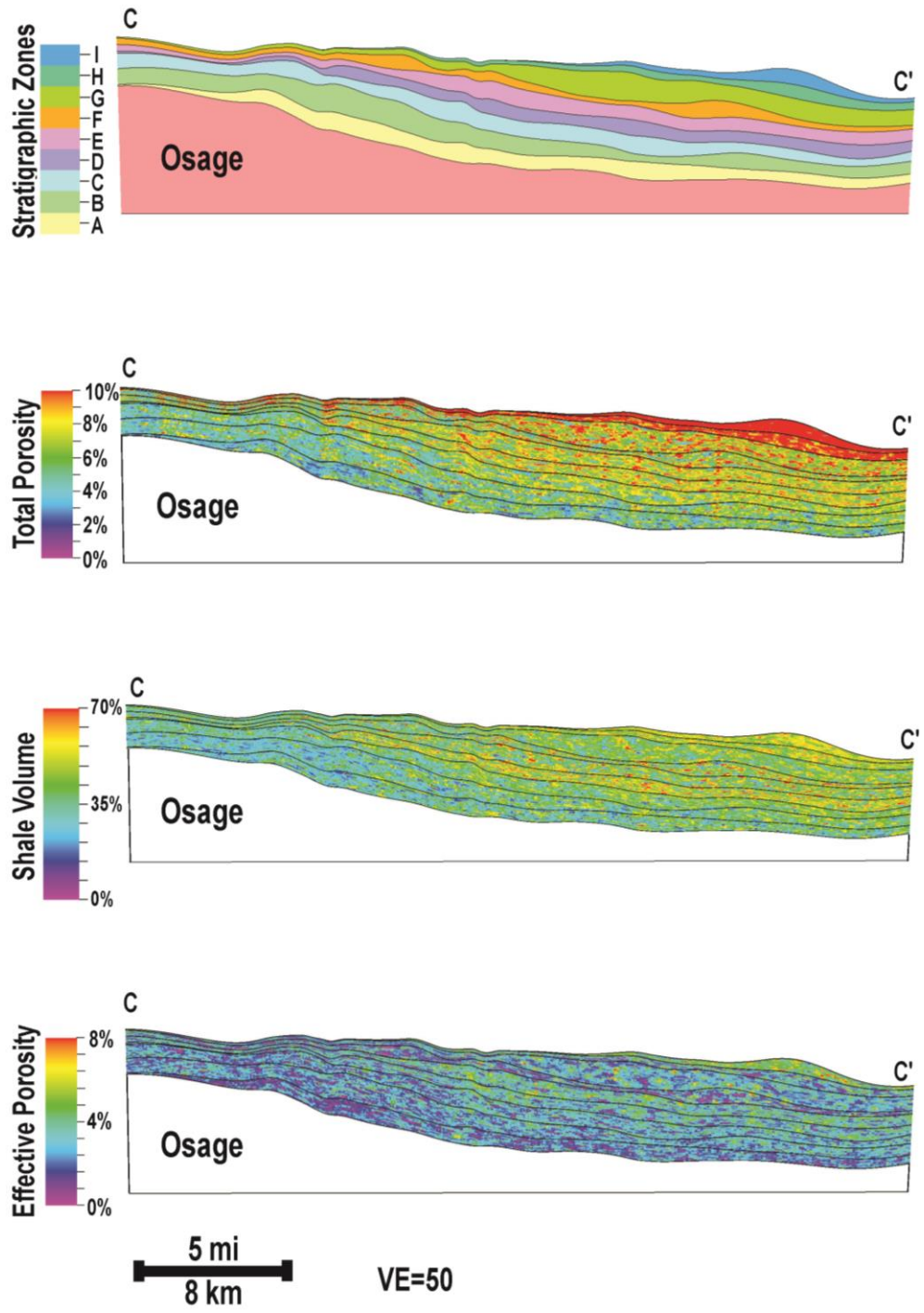
Figure 12. Cross-section C-C'. The stratigraphic framework, total porosity, shale volume, and effective porosity models are shown. Increasing V_{sh} values show a strong correlation to calculated Φ_T and Φ_E models increasing to the southeast. Model is flattened on the underlying Woodford shale.
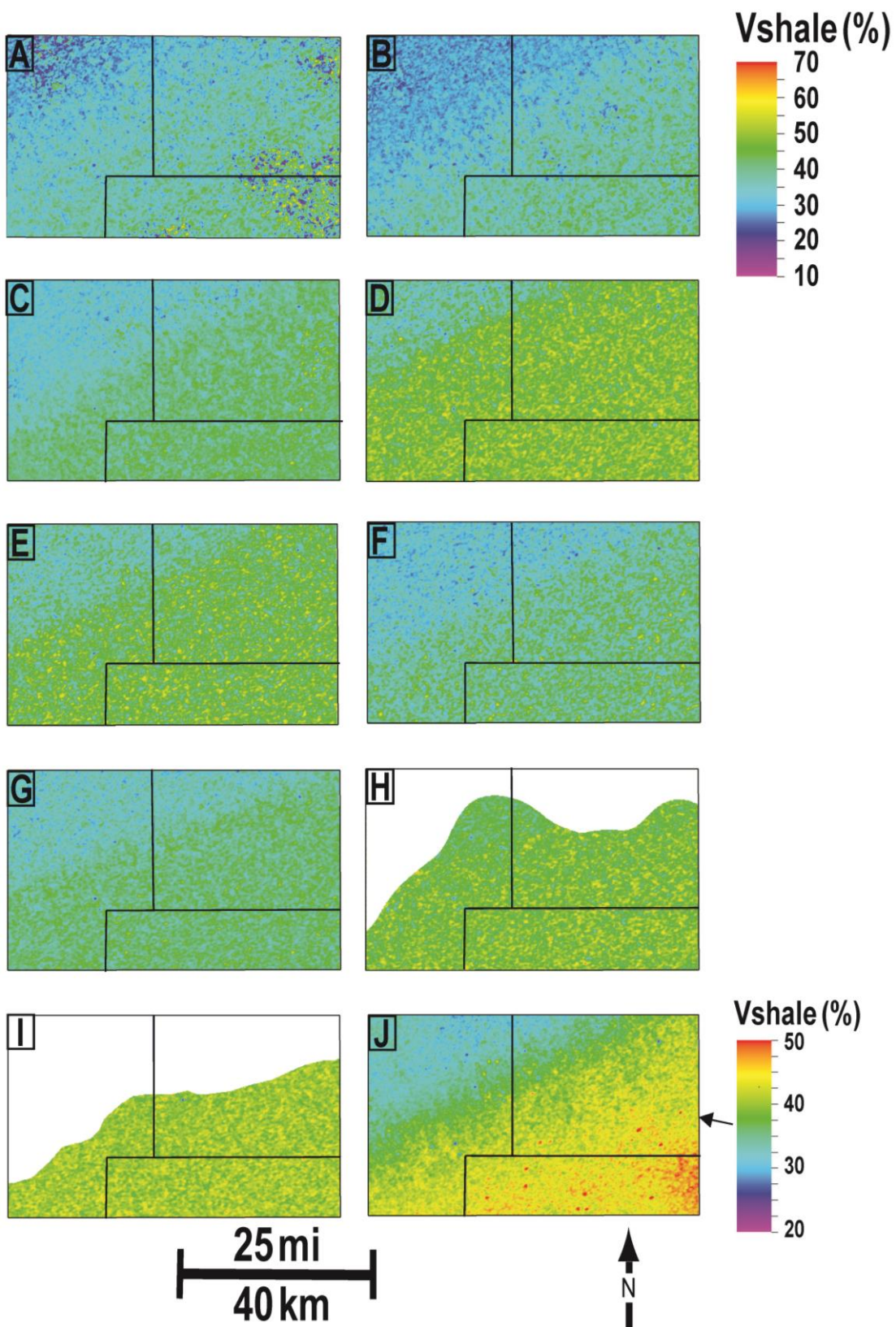
Figure 13. Mean V_{sh} maps calculated from the 3-D V_{sh} model. V_{sh} generally increases down-dip toward the southeast. A-I) Meramec parasequences A-I. J) Mean V_{sh} for the entire Meramec interval.
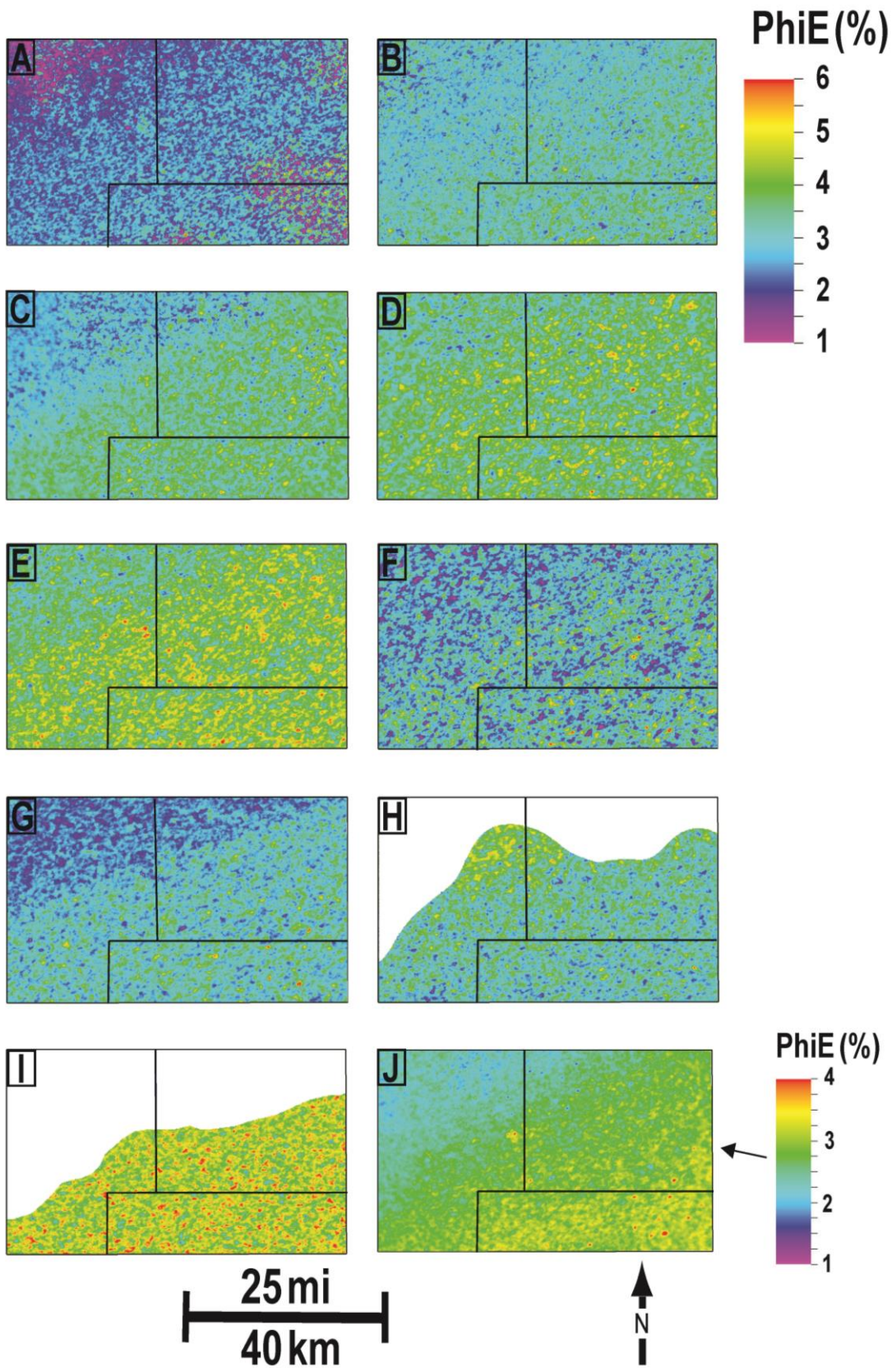
Figure 14. Mean Φ_E maps calculated from the 3-D model. Distributions of higher Φ_E correlate to V_{sh} trends (Figure 14) with increasing values to the southeast. A-I) Meramecian parasequences A-I. J) Mean Φ_E for the entire Meramecian interval.

Production Trends

Based on comparison of lithology and petrophysical property trends to production data (Figure 15), no clear relationships were identified. Given the large study area (1,050 mi^2 [~1,700 km^2]) and significant depth changes (-5580 to -11,825 ft [-1700 to -3600 km] SSTVD), it is likely that reservoir pressure and fluid properties in development areas exhibit significant controls on production values (Appendix G) independent from the varying lithology percentages in the wells.

Calculated 30-day GOR values ranging from 0.86 to 2.76 showed an expected trend of increasing GOR with reservoir depth. 30-day to 180-day percent GOR changes for the production wells shows a strong relationship between increasing reservoir depth and lower percent GOR change. Wells to the southwest where reservoir depth is greater exhibit 30 to 180-day percent GOR changes generally from 1-50%, while structurally up-dip wells GOR values changed up to 260% (Figures 16 and 17). This indicates changing reservoir pressure conditions with shallower, normally pressured wells being closer to the bubble point. Reservoir pressure conditions from initial to 180-day production volumes has a significant control on production volumes independent of lithology.

DISCUSSION

Depositional Environments

Meramec cored intervals in the Gulf Oil 1-23 Shaffer and Gulf Oil 1-25 Rohling contain 6 lithofacies with sedimentary structures that represent a wide range of depositional environments. Undulated bedding and mud wisps in the silty packstones and
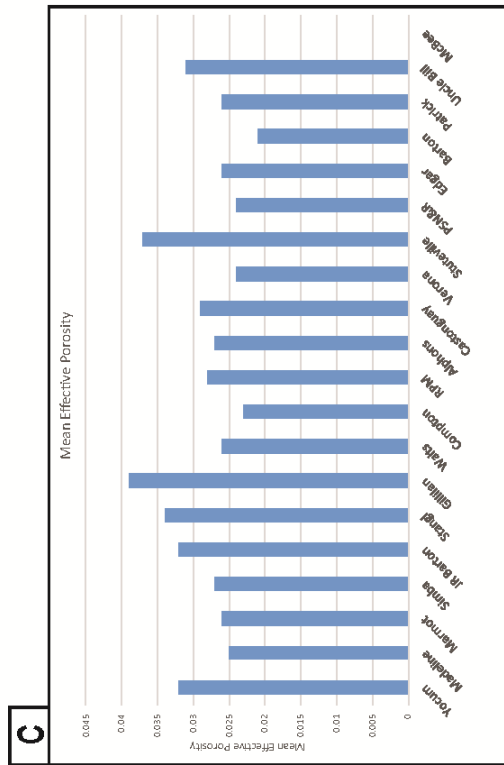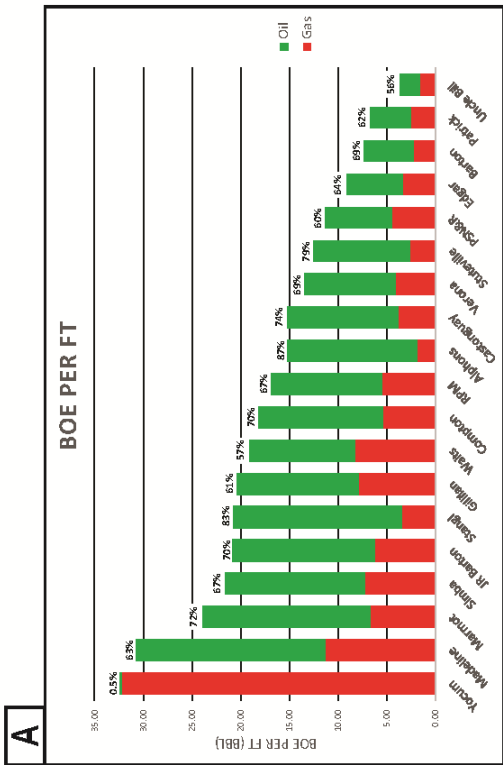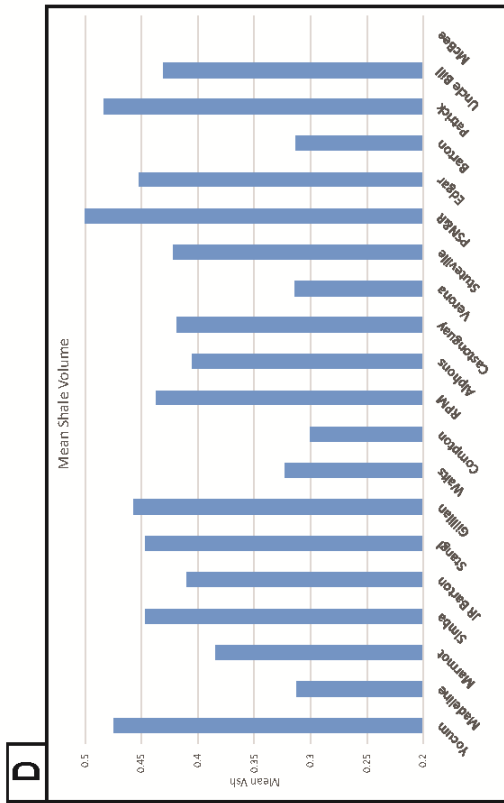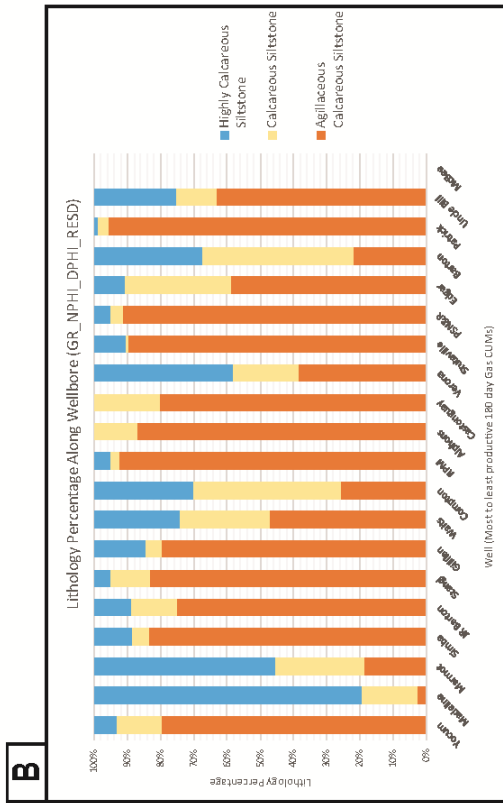
Figure 15. A) Graph of BOE/ft of lateral and percent oil vs percent gas for each production well. Wells are sorted from left to right from most to least productive. Percentages indicate percent oil of production B) Wells sorted most to least productive with lithology percentages calculated from synthetic logs from the horizontal wells. No distinct relationship between lithology and productivity is observed. C) Graph displaying mean effective porosity along the horizontal well from synthetic logs. D) Graph displaying mean V_{sh} along the horizontal wells. No distinct trend between productivity and petrophysical properties is observed.
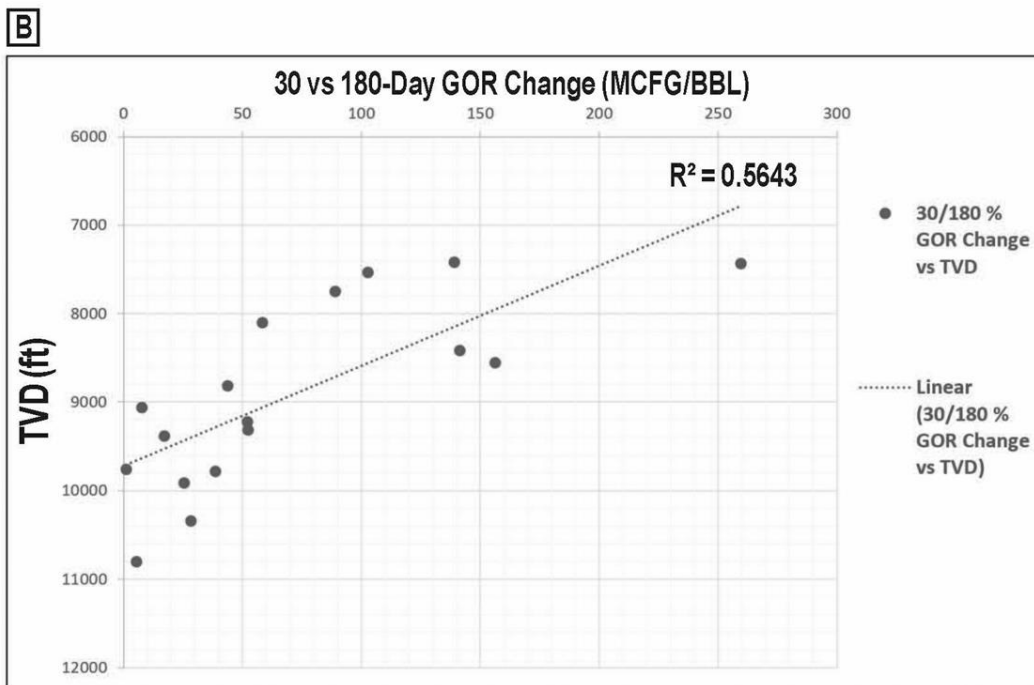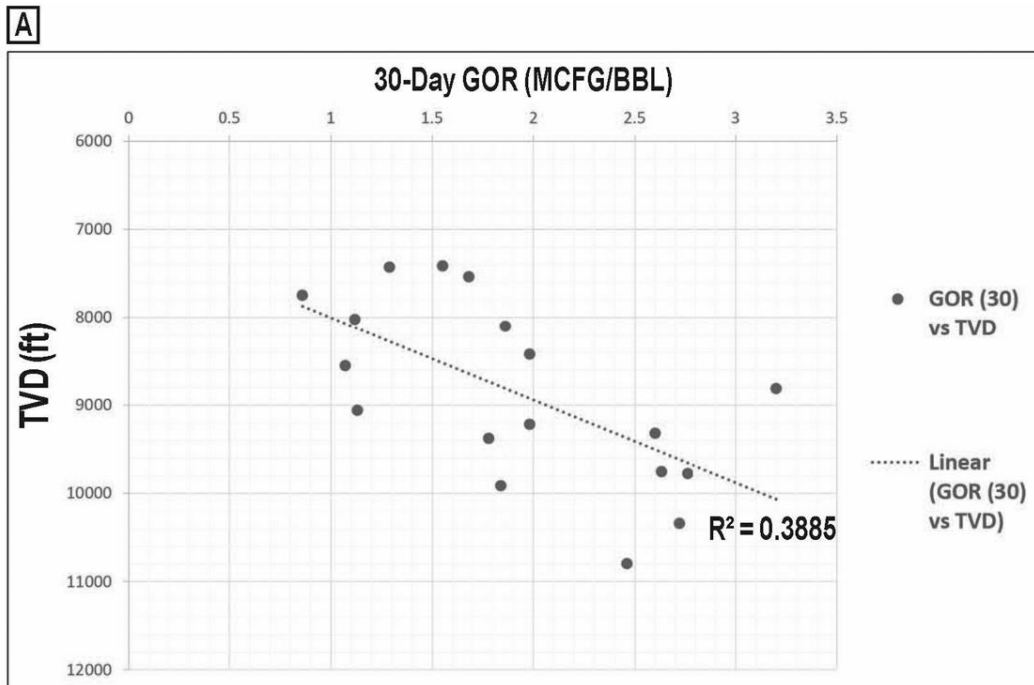
Figure 16. A) Graph of TVD (y-axis) vs. 30-day GOR (x-axis). A trend of increasing GOR from 0.8 to 3.32 is observed with increasing depth. B) TVD (y-axis) vs 30 to 180-day % GOR change. Deeper wells exhibit significantly higher % (up to ~250%) changes, indicating varying reservoir pressure with reservoir depth.
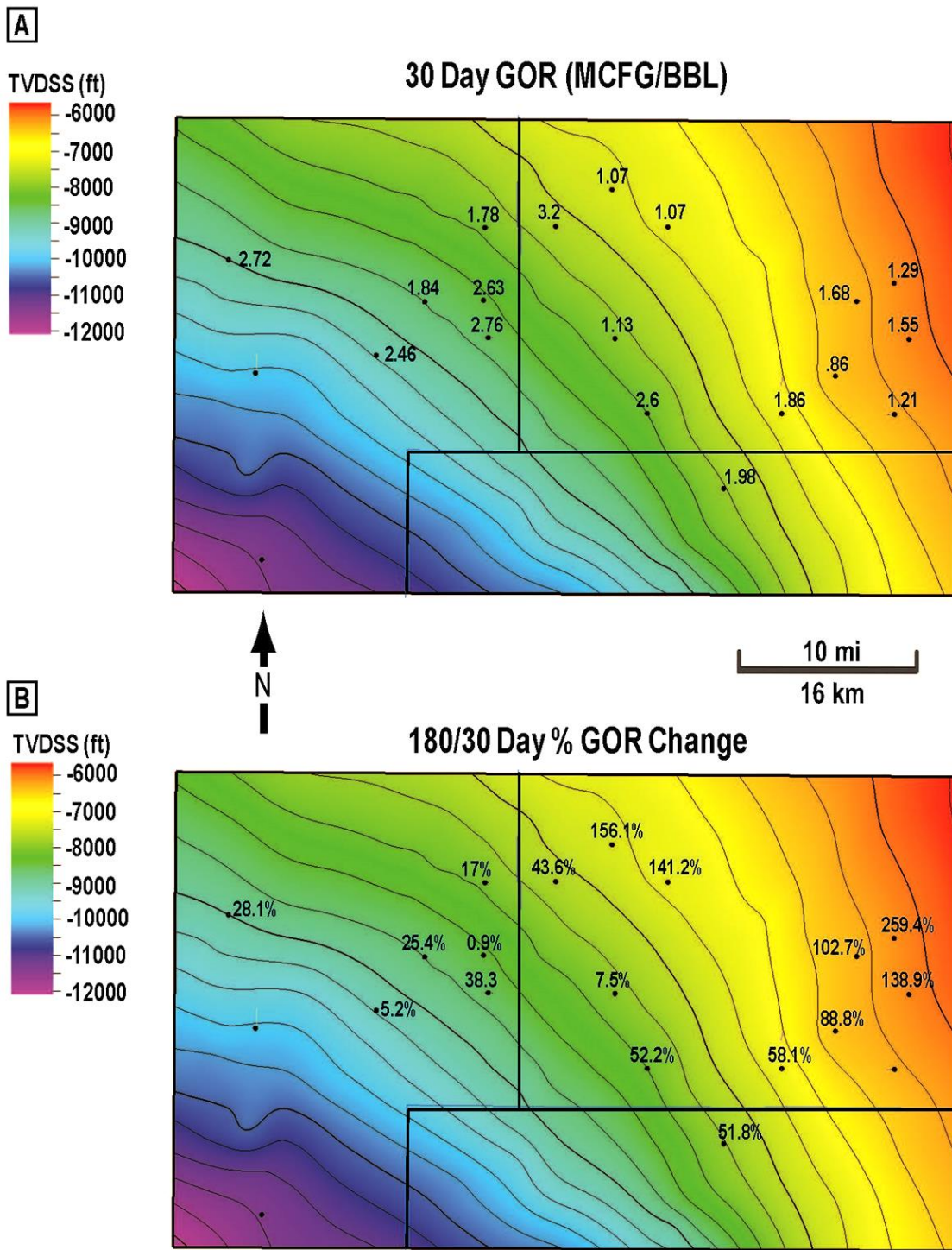
Figure 17. A) Map of 30-day GOR for production wells plotted on Meramec structure map. B) Map of 30 to 180-day % GOR change plotted on Meramec structure map.

grainstones were likely deposited in high energy, shallow water environments with significant tidal influence. Fossil fragments in these strata are typically reworked and irregular in bedding structure. This indicates they were likely deposited above fair-weather wave base in a lower shoreface to inner ramp environment where wave action was prevalent. Calcareous siltstones exhibit episodic occurrences of wavy and parallel laminations and varying amounts of calcite cement up to 70%. These deposits are interpreted to be an inner ramp facies variably in or around fair weather base. Calcite cementation is interpreted to be inversely correlated to interparticle clay abundance and primary depositional porosity. Therefore, facies deposited in higher energy, more proximal environments are more prone to occlusion of primary pore space and elevated diagenetic calcite-cement abundance. Bioturbated calcareous siltstones are dominantly structureless with some occurrences of hummocky cross-stratification. Some (<15%) interparticle clay and up to 40% calcite cement are observed with a primarily silt-sized quartz lithology. The presence of clays and less abundant stratification suggests this facies was deposited in a lower energy environment on the inner ramp, likely below fair-weather wave base. Increased clay content in the argillaceous calcareous siltstones represent facies deposited in lower energy environments. Intermittent intervals of laminated and bioturbated facies indicate this environment was likely within or below storm-wave base. The silty mudstone facies represents the lowest energy depositional environment and contain dominantly clay minerals. Some detrital silt-sized quartz and fossil fragments suggest this facies was not entirely deposited in the basin, but likely on

the outer ramp edge. Parasequences in the Meramec consist of facies successions from argillaceous lithologies to calcareous lithologies from bottom to top.

Stratigraphic Controls on Reservoir Quality

The primary goal of this study was to Reservoir quality in the Meramec is strongly controlled by the presence of some interparticle clays occluding calcite cementation. Higher mean Φ_E values are observed in areas with more abundant argillaceous lithologies. In addition to the higher reservoir storage potential, Cullen (2016) identified a strong correlation between core porosity and permeability in the Gulf Oil 1-25 Rohling and Gulf Oil 1-23 Shaffer wells. Therefore, vertical and lateral stratigraphic framework position is essential when determining reservoir quality in areas of development interest. Parasequences and reservoir targets deposited during a time of lower relative sea level are more likely to contain shallower lithologies with higher calcite abundances. Lithology classification models predict the highest abundance of argillaceous calcareous siltstone lithologies are present in the D and E parasequences bounded by the maximum flooding surface in the Meramec.

Price et al. (2017) also found that differing pressure gradients in the stacked reservoirs could indicate the presence of fracture barriers. He used a Diagnostic Fracture Injection Test (DFIT) and calculated Process Zone Stress (PZS) to conclude low porosity layers act as fracture barriers in the STACK. Given the multiple levels of cyclicity observed within the parasequences defined in this study, this emphasizes the importance

of additionally characterizing the stratigraphic architecture within each parasequence to determine optimal landing zones for a well.

CONCLUSIONS

The Mississippian Meramec in the STACK play consist of stacked carbonate and siliciclastic deposits that formed by multiple cycles of relative sea-level rise and fall within a low-order transgression. Reservoir quality is strongly controlled by the sequence stratigraphy of the interval. Key lithofacies include: 1) calcareous siltstones, 2) bioturbated calcareous siltstones 3) laminated argillaceous calcareous siltstones, 4) bioturbated argillaceous calcareous siltstones, 5) silty skeletal pack-grainstones, and 6) silty mudstones The lithofacies are grouped into 3 parent lithologies: 1) calcareous siltstones, 2) argillaceous calcareous siltstones, and 3) highly calcareous siltstones.

Lithology classifications using an ANN have cross-validation accuracies ranging from 88-91% in a training well and 73-83% in a testing well. Accuracy for lithology classification further away from cored wells decreased. This was interpreted to be due to changing lithology and fluid properties with distance from the cored wells used to train the ANN.

Φ_E is positively correlated to V_{sh}. It is interpreted that the presence of some clay will inhibit calcite cementation and preserve some primary porosity. Φ_E values range from 0-10% with an average of 2.5%. Values greater than 5% porosity were not observed in the cored wells. However, observations of core porosity measurements of up to 10%

from the Humble 1 Hawkins well in the southeastern distal portion of the study area qualitatively validate the occurrence of higher porosity in this area.

represented as northeast-southwest, strike elongate clinoforms. Lithology successions from argillaceous calcareous siltstones shallowing upward to highly calcareous siltstones compose the cycles. Sequences A-D make up a retrogradational sequence set capped by a maximum flooding surface for the Meramec. Subsequent parasequences E-G form a progradational package that progrades to the southeast. GRNORM logs in the H and I sequences indicate a final transgression in the later Meramec, resulting in an overall deepening of sea level. The parasequences represent a range of depositional environments from a lower shoreface to a distal shelf setting deposited over a low-gradient ramp. V_{sh} was observed to steadily increase to the southeast, indicating higher abundance of argillaceous lithologies and more calcareous lithologies towards the northwest in each parasequence set. Multiple levels of cyclicity were observed within the parasequences. The use of derivative trend analysis logs constructed from the GRNORM log assisted in accurate correlation of flooding surfaces at the scale of interest.

Lithology percentages from the models did not indicate production to be strongly controlled by lithology across the study area. GOR and reservoir pressure characteristics are associated with reservoir depth. It is likely variables such as completion techniques, reservoir pressure, and fluid properties likely exhibit stronger controls on production that the spatial variability of reservoir rock properties.

REFERENCES

Adler, F. J., 1971, Petroleum potential of the Anadarko basin and central Oklahoma area, AAPG Memoir 15, v. 2, p. 1061 – 1072.

Beebe, B. W., 1959, Characteristics of Mississippian production in the northwestern anadarko basin, Tulsa Geological Society Digest, V. 27, p. 190-205.

Birch, C. B., 2015, Reservoir-scale stratigraphy, sedimentology, and porosity characteristics of Mississippian reservoirs, northeastern anadarko shelf, Oklahoma, M.S. Thesis, University of Oklahoma, Norman, Oklahoma, 90 p.

Blakey, R., 2013, North American paleogeographic maps: Early Mississippian, 345 Ma: Website accessed March 20th, 2017, http://cpgeosystems.com/images/NAM_key-345Ma_EarM- sm.jpg

Campbell, J. A., C. J. Mankin, A. B. Schwarzkopf, and J. J. Raymer, 1988, Habitat of petroleum in Permian rocks of the midcontinent region; in, Permian Rock of the Midcontinent, W. A. Morgan and J. A. Babcock, eds.: Midcontinent Society of Economic Paleontologists and Mineralogists, Special Publication No. 1, p. 13-35

Cullen, A., 2017, Devonian-Mississippian petroleum systems of southern Laurasia: what make the STACK-Merge-SCOOP play in Oklahoma so special, AAPG Search and Discovery Article #10998,

Curtis, D. M., and S. C. Champlin, 1959, Depositional environments of Mississippian limestones of Oklahoma, Tulsa Geological Society Digest, V. 27, No. 1, p. 90-103.

Cronk, B. R., 2018, Development of unconventional reservoirs: fluid characterization, simulated reservoir volume determination, and production forecasting in the STACK, M.S. Thesis, University of Oklahoma, Norman, Oklahoma, 81 p.

Dutton, S. P., 1984, Fan-Delta Granite Wash of the Texas panhandle, Oklahoma City Geological Society, vol. Short Course Notes.

Flinton, K. C., 2016, The effects of high-frequency cyclicity on reservoir characteristics of the "Mississippian Limestone", Anadarko Basin, Kingfisher county, Oklahoma, M.S. Thesis, Oklahoma State University, Stillwater, Oklahoma, 412 p.

Frezon, S. E., and L. Jordan, 1979, Oklahoma, Paleotectonic investigations of the Mississippian system in the United States: U.S. Geological Survey Professional Paper 1010, p. 146-159.

Gallardo, J., and D. D. Blackwell, 1999, Thermal structure of the Anadarko basin, AAPG Bulletin, V. 83, No. 2, p. 333-361.

Grammer G. M., D. Boardman, J. Puckette, J. Gregg, J. Priyank., M. Childress, B. J. Price, B. Vanden Berg, and S. LeBlanc, 2013, Integrated reservoir characterization of Mississippian-age mid-continent carbonates: AAPG Search and Discovery Article #30297, 31 p.

Gutschick, R.C., and C. A. Sandberg, 1983, Mississippian continental margins of the conterminous United States, The Shelfbreak: Critical Interface on Continental Margins, SEPM Special Publication 33, p. 79-96.

Ham, W. E., R. E. Dension, and C. A. Merritt, 1965, Basement rocks and structural evolution of southern Oklahoma-a summary, AAPG Bulletin, V. 49, No. 7, p. 927-93

Haq, B. U. and S. R. Shutter, 2008, A chronology of Paleozoic sea-level changes: Science, vol. 322, p. 64-68.

Johnson, K. S. and K. V. Luza, 2008, Earth sciences and mineral resources of Oklahoma, Educational Publication 9, Oklahoma Geological Survey, 22 p.

Keller, G. R., and R. A. Stephenson, 2007, The southern Oklahoma aulacogen and Dniepr-Donets aulacogens: A comparative analysis, Geological Society of America Memoir 200, p. 127-143.

Lane, H. R., and T. L. De Keyser, 1980, Paleogeography of the late early Mississippian (tournaisian 3) in the central and southwestern United States, SEPM, Rocky Mountain Symposium 1, p. 149-162.

LeBlanc, S. E., 2014, High resolution sequence stratigraphy and reservoir characterization of the "Mississippian Limestone" in north-central Oklahoma, M.S. Thesis, Oklahoma State University, Stillwater, Oklahoma, 443 p.

Lindzey, K., 2015, Geologically constrained seismic characterization and 3-D reservoir modeling of Mississippian reservoirs, north-central Anadarko shelf, Oklahoma, M.S. Thesis, University of Oklahoma, Norman, Oklahoma, 106 p.

LoCricchio, E., 2012, Wash Play Overview, Anadarko Basin: Stratigraphic framework and controls on Pennsylvanian granite wash production, Anadarko

basin, Texas and Oklahoma, AAPG Search and Discovery Article, no. 110163.

Manger, W. L., 2011, Lower Mississippian sequence stratigraphy and depositional dynamics: insights from the outcrops, northwestern Arkansas and southwestern Missouri: Presentation, http://ogs.ou.edu/MEETINGS/Presentations/Miss2011/Manger.pdf (accessed February 25, 2017).

Mazzullo, S. J., 2011, Mississippian oil reservoirs in the southern Midcontinent: new exploration concepts for a mature reservoir objective: Search and Discovery Article #10373.

Mazzullo, S. J., B. W. Wilhite, D. R. Boardman, B. T. Morris., and C. J. Godwin, 2016, Stratigraphic architecture and petroleum reservoirs in lower to middle Mississippian strata (Kinderhookian to basal Meramecian) in subsurface central to southern Kansas and northern Oklahoma: Shale Shaker, vol. 67 no. 2, p. 20-49.

McConnell, D. A., M. J Goydas, G. N. Smith, and J. P. Chitwood, 1989, Morphology of the frontal fault zone, southwest Oklahoma: Implications for deformation and deposition in the Wichita uplift and Anadarko basin: Geology, v. 18, no. 7, p. 34-637.

Miller, J., 2018, Regional stratigraphy and organic richness of the Mississippian Meramec and associated strata, Anadarko basin, central Oklahoma, M.S. thesis, University of Oklahoma, Norman, Oklahoma, 154 p.

Northcutt, R. A., and J. A. Campbell, 1995, Geologic provinces of Oklahoma: Oklahoma Geological Survey Open-File Report 5-95, 1 sheet, scale 1:750,000, 6-page explanation and bibliography.

Parham, K. D., and R. A. Northcutt, 1993, Mississippian chert and carbonate and basal Pennsylvanian sandstone – central Kansas uplift and northern Oklahoma, D. Bebout, W. White, and T. Hentz, eds.: Atlas of major Midcontinent gas reservoirs, Austin, Bureau of Economic Geology, p. 57-59.

Perry, Jr., W. J., 1990, Tectonic evolution of the Anadarko basin region, Oklahoma, U.S. Geological Survey Bulletin 1866-A, p. A1-A19.

Pranter, M. J., A. M. Turnini, K. J. Marfurt, and D. Devegowda, 2016, Multidisciplinary characterization and modeling of Mississippian carbonate and silica-rich reservoirs, northern Oklahoma, AAPG Mid-continent Section Meeting, Tulsa, Oklahoma, October 4-6, 2015, AAPG Search and Discovery #51231.

Price, B., K. Haustveit, and A. Lamb, 2017, Influence of stratigraphy on barriers to fracture growth and completion optimization in the Meramec Stack Play, Anadarko Basin, Oklahoma: Unconventional Resources Technology Conference (URTEC), Article #2697585, 8 p.

Pyrcz, M. J., and C. V. Deutsch, 2014, Geostatistical reservoir modeling, 2nd ed. New York, Oxford University Press p. 122-127, 228-244.

Rowland, T. L., 1961, Mississippian rocks in the subsurface of the Kingfisher-Guthrie area, Oklahoma, Oklahoma City Geological Society, The Shale Shaker Digest IV, V. 12-14, p. 145-162

Shapiro, L.G., and G. C. Stockman, 2000, Computer vision: Upper Saddle river, NJ, Prentice Hall, p.170

Shelly, S., M. G. Grammer, and M. J. Pranter, 2017, Reservoir characterization and modeling of a subsurface Meramec analog from a quarry in northeastern Oklahoma, Shale Shaker: Oil and Gas Exploration, Vol. 68 No. 5, p. 224-242.

Sloss, L. L., 1963, Sequences in the cratonic interior of north america, Geological Society of America Bulletin, V. 74, No. 2, p 93-114.

Turnini, A. M., 2015, Stratigraphic and structural controls on Mississippian limestone and tripolitic chert reservoir distribution using seismic-constrained reservoir characterization and modeling, northern Oklahoma, M.S. Thesis, University of Oklahoma, Norman, Oklahoma, 83 p.

Watney, W. L., W. J. Guy, and A. P. Bynes, 2001, Characterization of the Mississippian chat in south-central Kansas: AAPG Bulletin, vol. 85, p. 85-113

Wethington, N., 2017, Stratigraphic architecture of the Mississippian limestone through integrated electrofacies classification, Hardtner field area, Kansas and Oklahoma, M.S. Thesis, University of Oklahoma, Norman, Oklahoma

Wickham, J. S., 1978, The southern Oklahoma aulacogen, Geological Society of America, In structural style of the Arbuckle region, South-Central section guidebook for field trip 3, p. 9-41.

APPENDIX

LIMITATIONS

This section addresses some of the results and potential sources of error associated with the methods used, and recommended data and methods that could be implemented to improve the results.

Artificial Neural Networks

Lithologies were classified in non-cored wells using a supervised ANN with a suite of well logs (GRNORM, NPHI, DPHI, and RESD).

This study used two wells < 1 mi (<1 km) apart with partial cored intervals in each (Gulf Oil 1-25 Rohling and Gulf Oil 1-25 Shaffer). In the Gulf Oil 1-25 Rohling "training" well, the lower to middle Meramec was cored and used to train the estimation models. For the Gulf Oil 1-23 Shaffer "testing" well, the middle to upper Meramec was used to test the resulting accuracies of the estimations made by the ANN (Figure 3). The observed stratigraphic variability of the interval leads to the assumption that lithofacies in the training and testing wells are likely significantly different, thus leading to the construction of lithology logs based on lithology. A similar methodology using fully cored Meramec interval with ample XRD and thin section photomicrographs could potentially yield more accurate results.

Classification accuracies achieved in the nearby "testing" well were reasonable (state the percentages again here). However, given that the geology of the Meramec interval changes significantly across this 1,050 mi^2 (~1,700 km^2) area, there are

limitations associated with estimating lithology in wells farther away from the training wells.

To test the distance limitations of classifications, lithologies were classified in a non-disclosed cored well approximately 7 mi (11 km) from the training well (Appendix C). The GR curve for the well was normalized with the GRNORM data set for the 175 wells with wireline log data. Overall accuracy was 55% for the ANN classification model indicating that within this distance decreased accuracy can be expected. Accuracy for the argillaceous lithologies was 71%. However, classification accuracy of the calcareous and highly calcareous lithologies declines significantly (16% and 53% respectively). Changing lithology and fluid properties with distance from the training well can potentially impact the effectiveness of the classification method.

Examples of argillaceous lithologies misclassified as highly calcareous siltstones can be observed to the southeast primarily in parasequences H and I (Appendix C). GRNORM profiles in these intervals exhibit relatively high values, indicating a high abundance of clay and likely low abundance of calcite cement associated with distal shelf to basinal depositional environments. ANN classifications in this interval consisted of almost entirely highly calcareous siltstone generally associated with lower shore-face, and inner shelf, calcite-rich, and clay-poor rocks. The misclassification is likely a combination of neither of these intervals being cored or used in the training or testing of the ANNs, and the significant distance (>15 mi [>24 km]) from the cored well locations. Results could be improved with additional core data with better spatial sampling.

Petrophysical Calculations

Φ_E calculations are consistent with core-measured porosity (Figure 5). Shelly et al. (2017) and Cullen (2017) observed a strong relationship between core porosity and permeability in the Meramec interval (Appendix D). Φ_E is also positively correlated with V_{sh} and this is consistent with observations of Price et al. (2017) and Shelly et al. (2017). While core porosity from the Humble 1 Hawkins well in the southeast (Figure 4) qualitatively validated the Φ_E calculations (Appendix D), well-log data for this well are not available to quantitatively compare to core porosity (Appendix D). Additional core-derived porosity and associated well-log data for more wells is required to quantitatively validate the usefulness of this empirical method.

Production Wells

Detailed reservoir fluid/pressure studies could result in a better understanding of geologic controls of well performance. In "tight rock" reservoirs, completion techniques are also a key factor in the productivity of a well. Variables such as fracture lengths, fracture heights, well-spacing per section, and proppant types can have a significant impact on the production performance.

DETAILED FACIES DESCRIPTIONS

Facies 1 (Figure 7A and 8A) is a light grey, dominantly structureless, calcareous siltstone composed of well-sorted, sub-rounded to sub-angular, silt-sized quartz grains. Intergranular calcite-cement is present in varying abundances ranging from 15 – 65%. Wavy and horizontal laminations are well defined, faint, or non-existent in discreet units. Laminations are sometimes disrupted by light horizontal to sub-vertical bioturbation. In the structureless intervals, calcite-filled vertical fractures are prominent.

Facies 2 (Figure 7B and 8B) is a light grey calcareous siltstone composed of well-sorted, sub-rounded to sub-angular silt-sized quartz grains and sparse amounts of dark, clay-filled burrows (15%). Intergranular calcite-cement within the quartz grains in non-burrowed areas is prominent. Some faint laminations are observed in these intervals.

Facies 3 (Figure 7C and 8C) is a medium to dark grey argillaceous calcareous siltstone composed of well-sorted, sub-rounded to sub-angular silt-sized quartz grains with dominant wavy, horizontal, and hummocky laminations composed of clay minerals (>15%). Intergranular calcite cement is still present but in lesser amounts than facies 1 and 2 owing to the increased occurrence of intergranular clay particles.

Facies 4 (Figure 7D and 8D) is a medium to dark grey argillaceous calcareous siltstone composed of well-sorted, sub-rounded to sub-angular silt-sized quartz grains with abundant dark, clay-filled burrows (>20%). Calcite-cement is present but significantly decreased likely owing to the elevated amounts of intergranular clay minerals hindering the formation of calcite (Price et al., 2017).

Facies 5 (Figure 7E and 8E) is a light grey highly calcareous (<50%) pack-grainstone carbonate with abundant peloids and calcite cement, mud wisps, various amounts of fossil fragments, and sparse amounts (15%) of scattered, well-sorted, silt-sized quartz grains. Fossils fragments are dominated by crinoid beds with some bivalves, brachiopods, and bryozoans observed in discrete lenses. Calcite cement commonly nucleates around fossil grains.
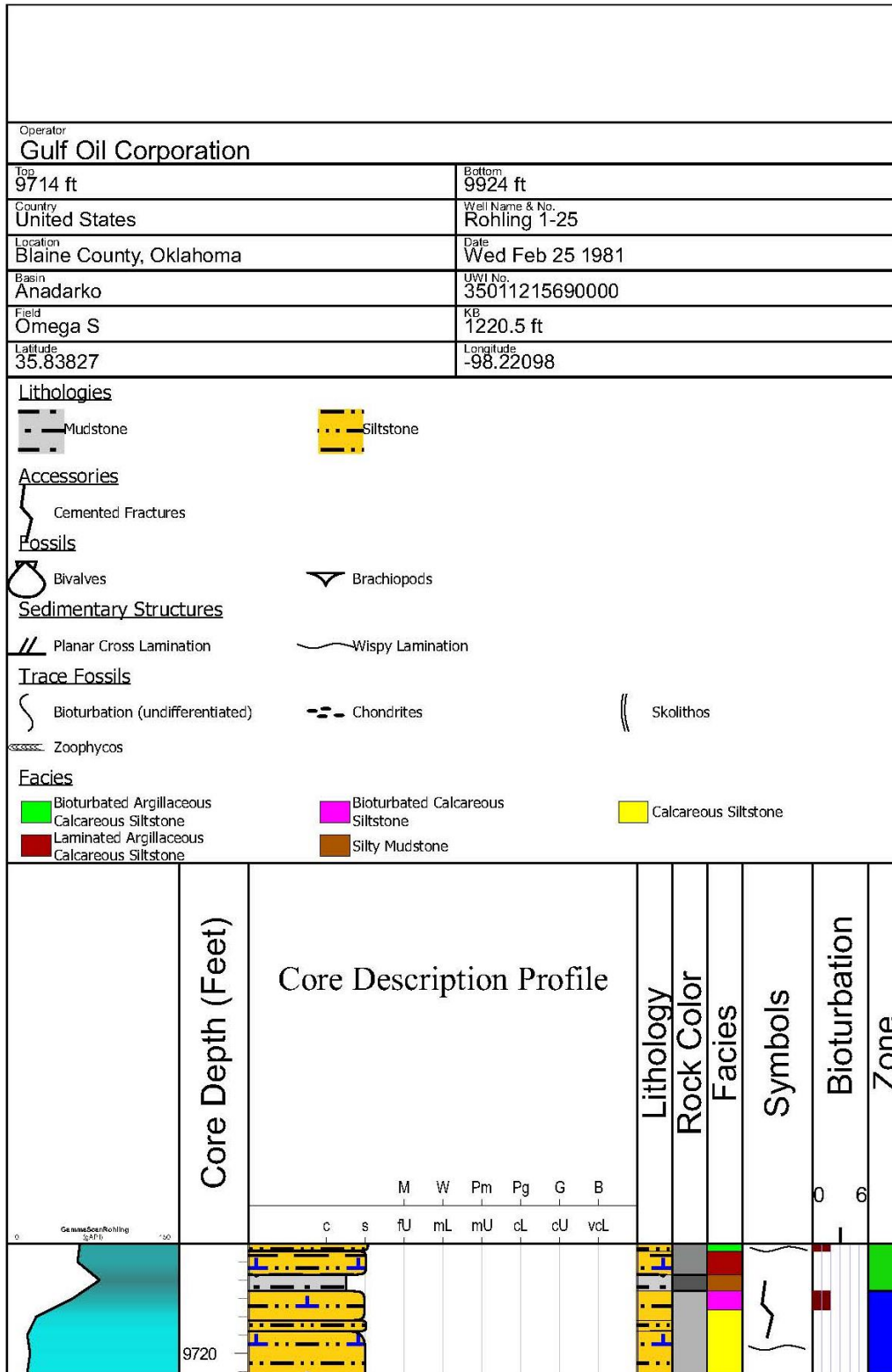
Facies 6 (Figure 7F and 8F) is a dark grey structureless to lightly laminated silty mudstone with some calcite-cement (<15%) and decreased levels of well-sorted, sub-rounded to sub-angular silt-sized quartz grains. Light to moderate bioturbation and occasional brachiopod and bivalve shell fragments are observed in some intervals.
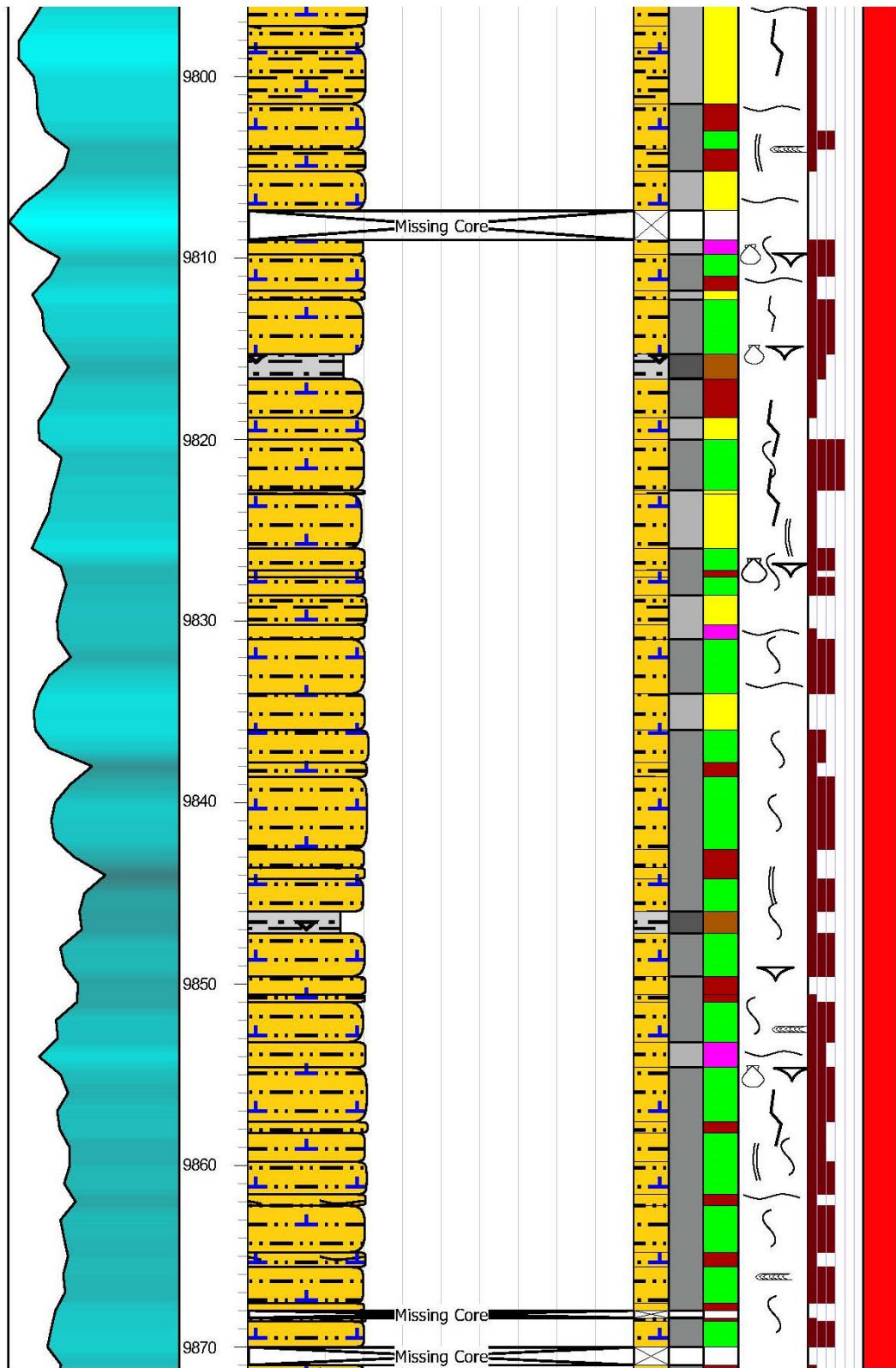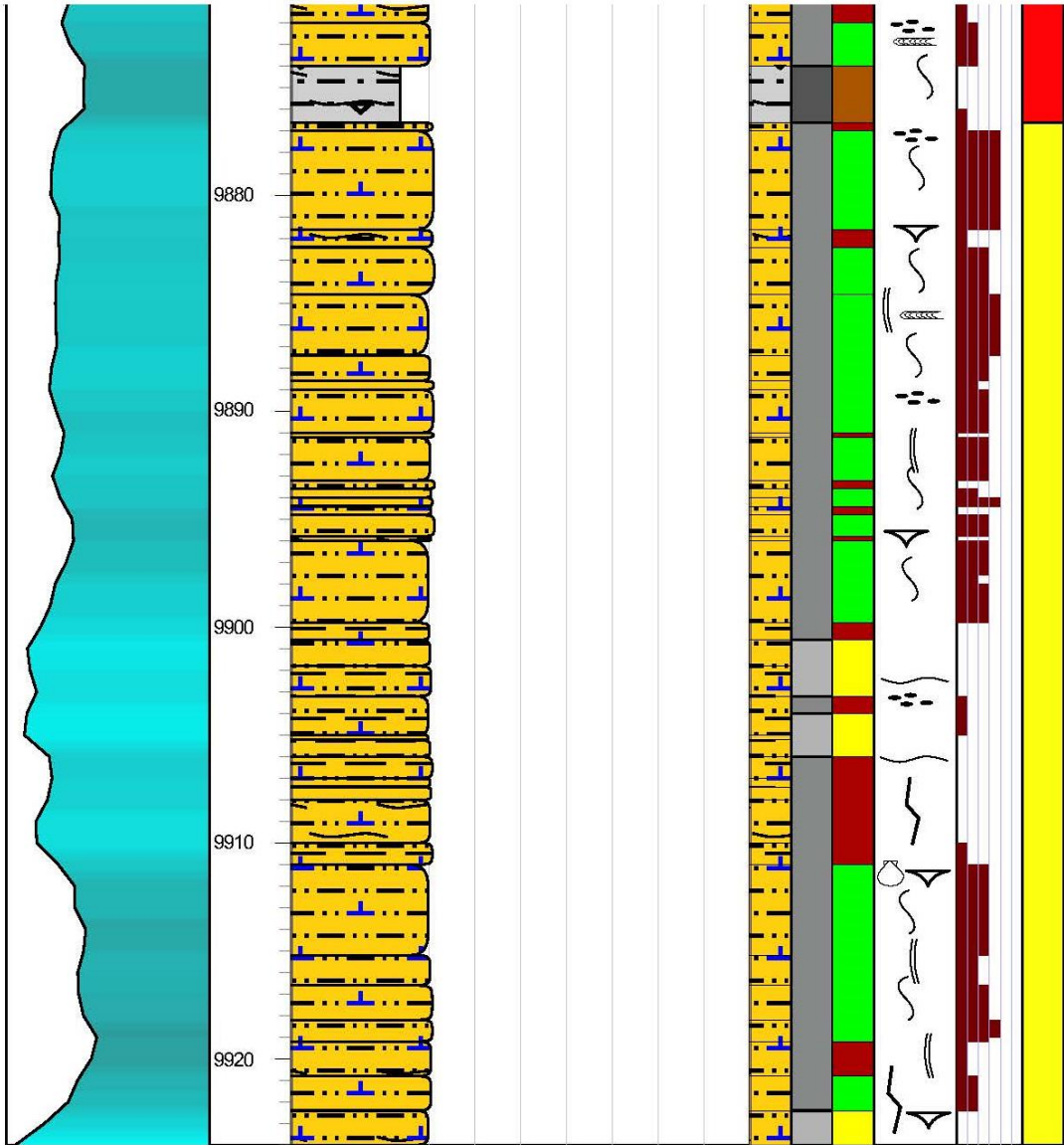
Appendix A – Geologic Setting
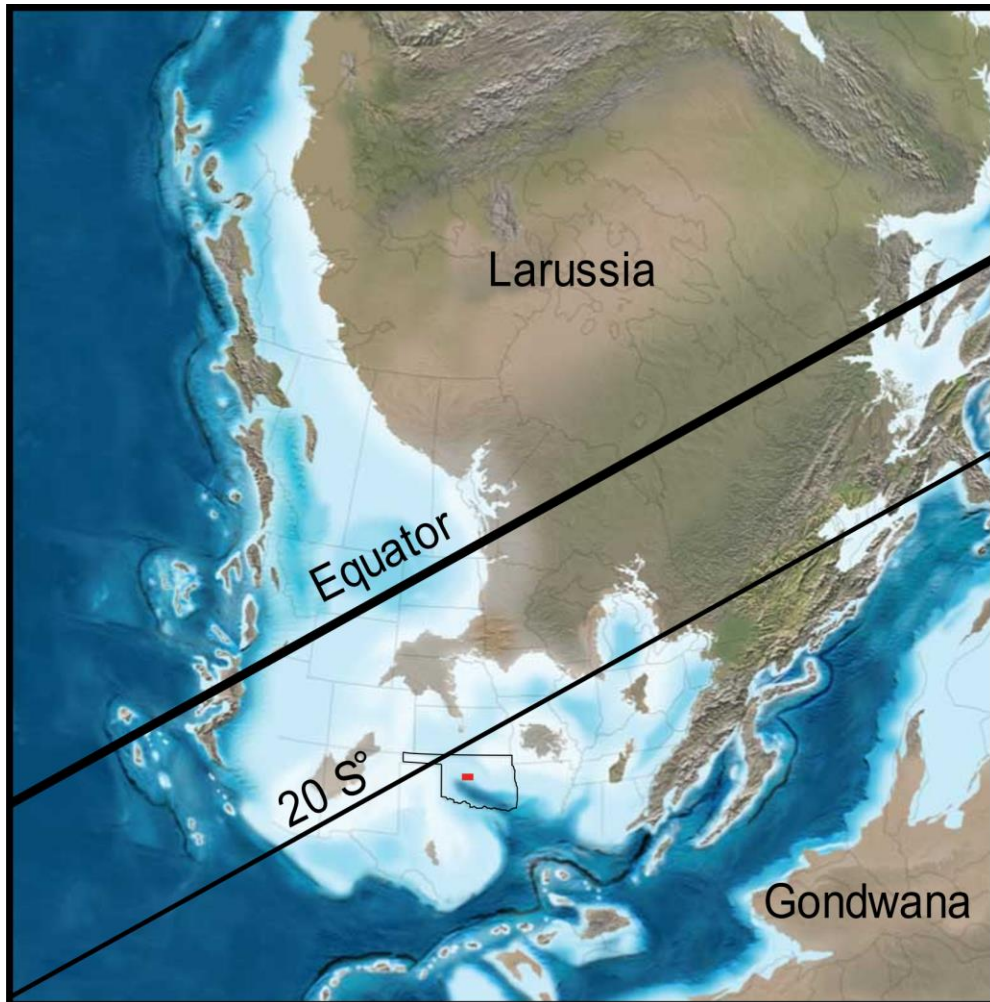
Appendix A-1. Paleogeography of the early Mississippian. The study area is located on the margin of the Anadarko Basin on a widespread carbonate ramp in a humid to sub-tropical environment around 25° latitude (Curtis and Champlin, 1959). (Modified from Blakey, 2013 and Flinton, 2016).
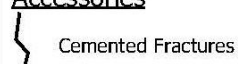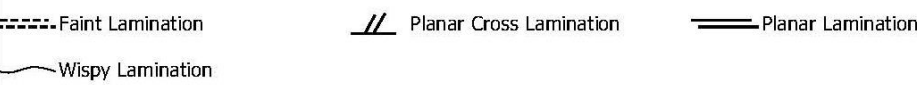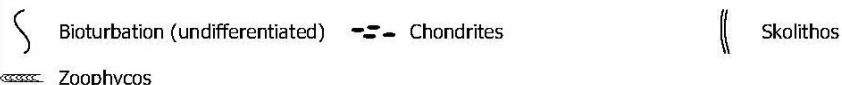
Appendix B – Core Descriptions

Missing Core

Missing Core

Missing Core

Missing Core

Missing Core

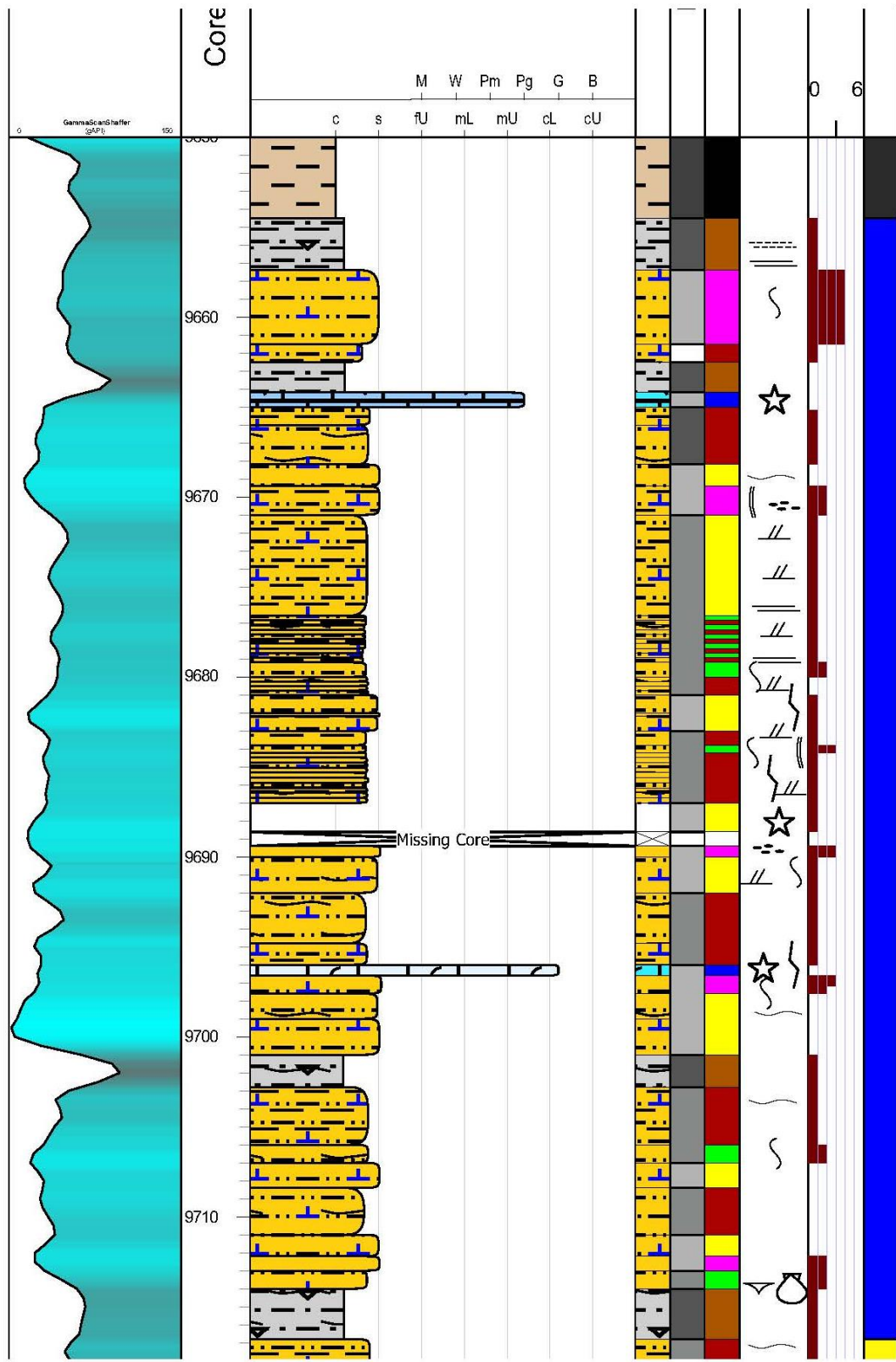Missing Core

Operator	
Gulf Oil Corporation	
Top 9650 ft	Bottom 9887 ft
Country United States	Well Name & No. Shaffer 1-23
Location Blaine County, Oklahoma	Date Sat Aug 30 1980
Basin Anadarko	UWI No. 35011215220000
Field Omega W	KB 1250 ft
Latitude 35.84283	Longitude -98.23551

Lithologies

Claystone Limestone Mudstone

Sandstone Siltstone

Accessories

Cemented Fractures

Fossils

Bivalves Brachiopods Crinoids

Sedimentary Structures

Faint Lamination Planar Cross Lamination Planar Lamination

Wispy Lamination

Trace Fossils

Bioturbation (undifferentiated) Chondrites Skolithos

Zoophycos

Facies

Bioturbated Argillaceous Calcareous Siltstone Bioturbated Calcareous Siltstone Calcareous Siltstone

Laminated Argillaceous Calcareous Siltstone None Shale

Silty Mudstone Silty Pack-Grainstone

Depth (Feet)	Core Description Profile	Lithology	Rock Color	Facies	Symbols	Bioturbation	Zone

9870

9880

Missing Core

Appendix C – Lithology Classifications

ANN 1 Predicted Lithologies 88% Accuracy	Actual Lithologies		
	Calcareous Siltstone (1)	Argillaceous Calcareous Siltstone (2)	Heavily Calcareous Siltstone (3)
1	14	0	0
2	4	158	7
3	11	12	81
User's Accuracies	48%	93%	92%

ANN 2 Predicted Lithologies 91% Accuracy	Actual Lithologies		
	Calcareous Siltstone (1)	Argillaceous Calcareous Siltstone (2)	Heavily Calcareous Siltstone (3)
1	20	0	4
2	2	165	9
3	7	5	75
User's Accuracies	69%	97%	85%

ANN 3 Predicted Lithologies 91% Accuracy	Actual Lithologies		
	Calcareous Siltstone (1)	Argillaceous Calcareous Siltstone (2)	Heavily Calcareous Siltstone (3)
1	17	0	0
2	4	166	11
3	8	4	77
User's Accuracies	59%	98%	88%

ANN 3 Predicted Lithologies 91% Accuracy	Actual Lithology		
	Calcareous Siltstone (1)	Argillaceous Calcareous Siltstone (2)	Heavily Calcareous Siltstone (3)
1	17	0	0
2	4	166	11
3	8	4	77
User's Accuracies	59%	98%	89%

Appendix C-1. ANN accuracies in the Gulf Oil 1-25 Rohling training well. A) ANN 1 inputs: GRNORM, DPHI, RESD. B) ANN 2 inputs: GRNORM, DPHI, RHOB. C) ANN 3 inputs: GRNORM, NPHI, DPHI, RESD. D) ANN 4 inputs: GRNORM, DPHI, NPHI.

ANN 1 Predicted Lithologies 83% Accuracy	Actual Lithologies		
	Calcareous Siltstone (1)	Argillaceous Calcareous Siltstone (2)	Heavily Calcareous Siltstone (3)
1	0	2	6
2	6	77	3
3	11	4	77
User's Accuracies	0%	93%	90%

ANN 2 Predicted Lithologies 48% Accuracy	Actual Lithologies		
	Calcareous Siltstone (1)	Argillaceous Calcareous Siltstone (2)	Heavily Calcareous Siltstone (3)
1	5	17	57
2	3	66	10
3	9	0	19
User's Accuracies	29%	80%	22%

ANN 3 Predicted Lithologies 80% Accuracy	Actual Lithologies		
	Calcareous Siltstone (1)	Argillaceous Calcareous Siltstone (2)	Heavily Calcareous Siltstone (3)
1	9	3	15
2	1	72	3
3	7	8	68
User's Accuracies	53%	93%	90%

| ANN 4 Predicted Lithologies 73% Accuracy	Actual Lithologies		
	Calcareous Siltstone (1)	Argillaceous Calcareous Siltstone (2)	Heavily Calcareous Siltstone (3)
1	5	0	16
2	10	64	4
3	2	19	66
User's Accuracies	0%	93%	90%

Appendix C-2. ANN accuracies in the Gulf Oil 1-23 Shaffer testing well. A) ANN 1 inputs: GRNORM, DPHI, RESD. B) ANN 2 inputs: GRNORM, DPHI, RHOB. C) ANN 3 inputs: GRNORM, NPHI, DPHI, RESD. D) ANN 4 inputs: GRNORM, DPHI, NPHI.
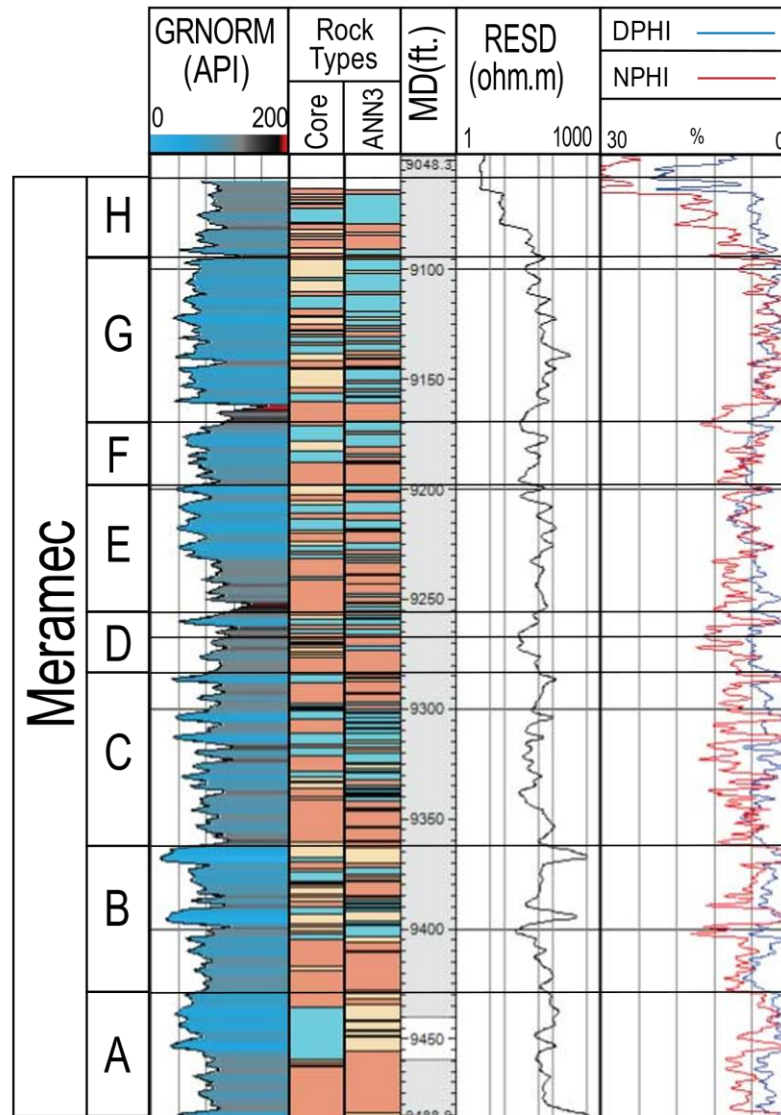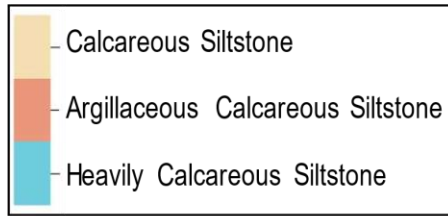
Appendix C-3. Rock type estimations within an undisclosed well within ~10 mi. (16 km.) of the cored wells used to train the ANN. Misclassifications can be observed, particularly between the calcareous siltstone and heavily calcareous siltstone rock types, can be observed within this distance. This poses limitations on the size of an area of interest that can be modeled using this estimation technique.

Predicted Lithologies 55% Accuracy	Actual Lithology		
	Calcareous Siltstone (1)	Argillaceous Calcareous Siltstone (2)	Heavily Calcareous Siltstone (3)
1	28	37	59
2	57	311	52
3	95	87	127
User's Accuracies	16%	71%	53%

Appendix C-4. Confusion matrix of the accuracy of rock type estimations using ANN 3 in the undisclosed cored-well. Estimations of the argillaceous rock types maintain a reasonable accuracy (71%), while uncertainty between the calcareous rock type decrease significantly (13% and 53%). This results in an overall accuracy of 55%. Misclassifications could be a results of varying fluid properties in the reservoirs resulting in different log responses for respective rock types.
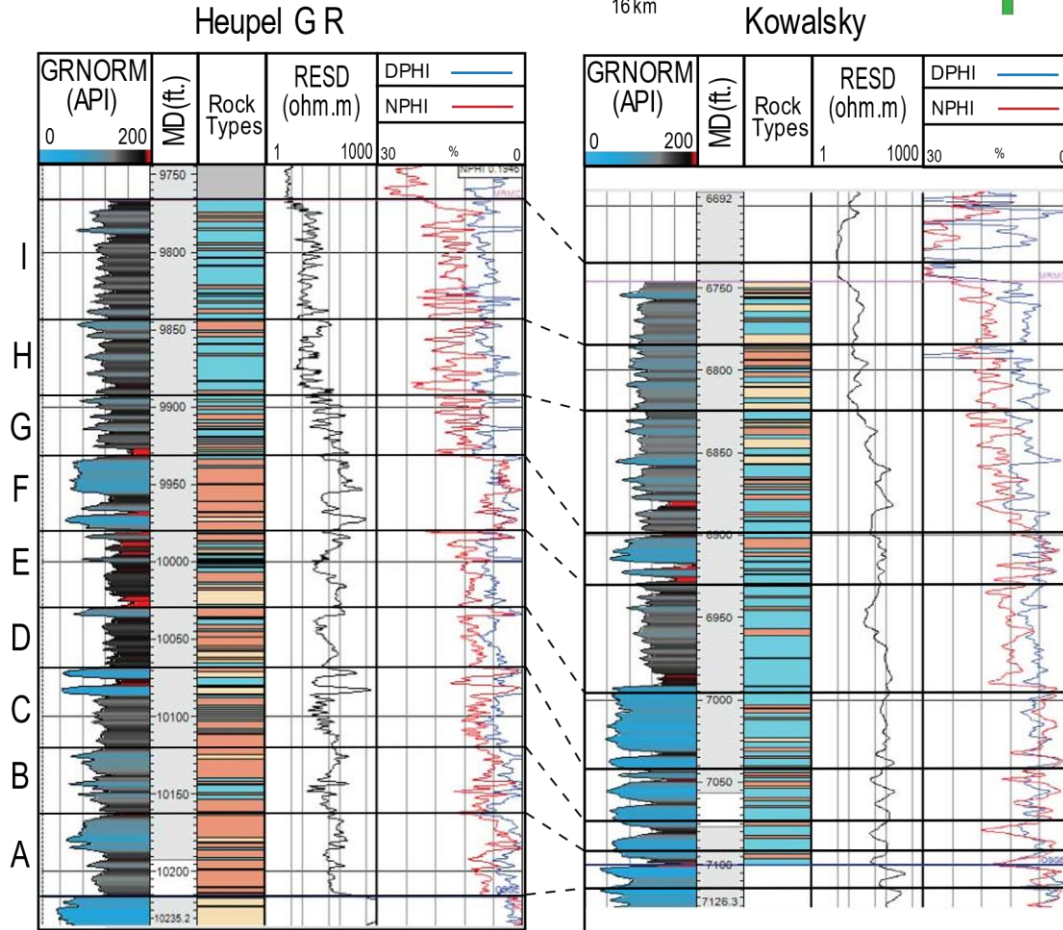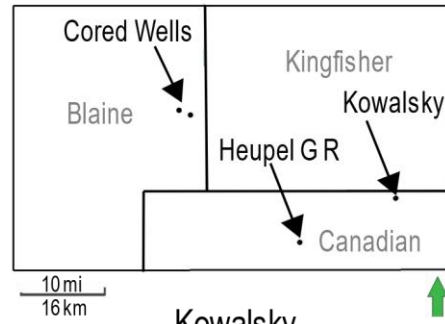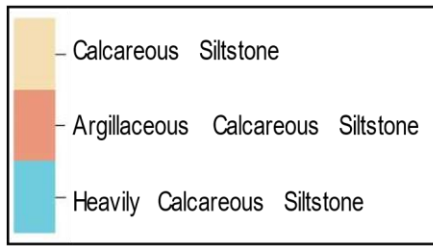
Appendix C-5. Example of misclassification of rock types in the far southeast of the study area. Zones associated with high GRNORM values indicating clay-rich intervals are classified as highly calcareous siltstone rock types. This indicates an increasing uncertainty in estimations with distance from the location of the ANN training.

Appendix D – Petrophysical Calculations

Core Porosity vs. Log-based Porosity							
Gulf Oil 1-23 Shaffer				Gulf Oil 1-25 Rohling			
Depth (MD)	Porosity (%)	Log Φ_T	Log Φ_E	Depth (MD)	Porosity (%)	Log Φ_T	Log Φ_E
96661	2.04	2.9	0.4	97085	2.07	7.6	2.9
96808	0.74	4.8	1.1	97362	2.50	5.9	2.6
96988	0.79	3.0	0.6	97372	1.67	5.3	0.6
97018	2.78	5.0	0.1	97658	1.84	6.5	1.8
97135	3.06	7.4	1.3	97038	2.02	7.0	2.2
97275	3.43	6.8	3.5	98139	1.87	4.1	2.0
97528	2.41	6.8	2.0	98344	0.76	4.4	1.1
97805	0.99	4.9	1.5	98448	2.42	9.0	3.5
97895	2.68	7.9	3.5	98796	0.75	4.7	1.8
98143	2.08	5.9	0.9	98935	0.63	3.8	0.6
98395	2.19	7.3	1.7	99039	1.38	2.0	0.3
98435	0.32	1.8	0.1	99074	0.42	3.3	1.4
98690	3.03	7.2	3.2				
98870	3.80	10.0	4.9				

Appendix D-1. Core measured porosity values in the Gulf Oil 1-23 Shaffer and Gulf Oil 1-25 Rohling cored-wells used to compared calculated values to cored-derived porosity.

Humble #1 Hawkins		
Sample #	Depth	Core Porosity
1	7738.60	0.3
2	7741.20	2.1
3	7757.8	0.8
4	7771.2	1.5
5	7778	1.7
6	7780.4	5.8
10	7811.1	6.0
11	7820.1	5.1
12	7822.8	5.5
13	7826.5	2.0
14	7835	5.4
15	7836.7	1.4
16	7844.2	3.1
17	7865.3	3.5
18	7873.9	2.2
19	7891.6	1.0
20	7898.9	0.7
21	7908.8	0.2
22	7916.1	9.5
23	7916.8	7.1
25	7926.6	2.1
26	7936.6	3.8
27	7945.1	0.6
28	7948.6	7.2
29	7952.1	1.4
30	7954.3	0.1
31	7958.2	4.9
32	7959.3	1.1
33	7963.9	3.6
35	7972.2	3.9
36	7979.7	2.3
37	7984.1	1.2
38	7986.7	8.1
39	7991.6	6.5
40	7998.5	0.4
41	8006.1	1.8

Appendix D-2. Core derived porosity values in the cored-well without LAS data (Figure 3). Measured values up to 9.5% support the validity of log calculations indicating increasing porosity basin-ward (Figure 14).
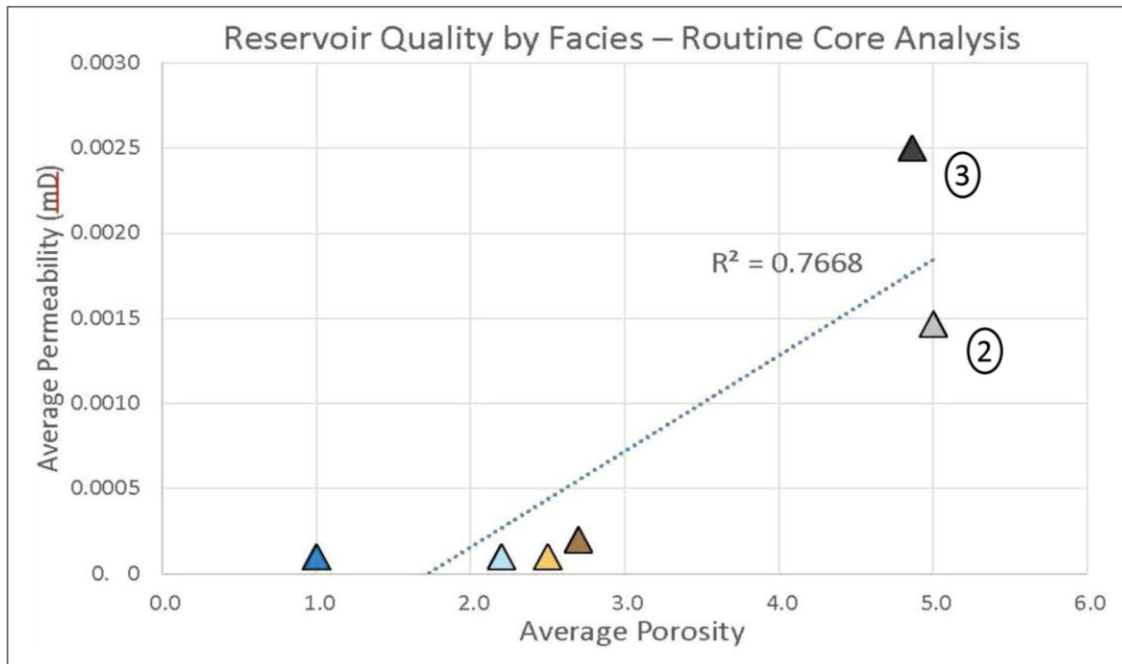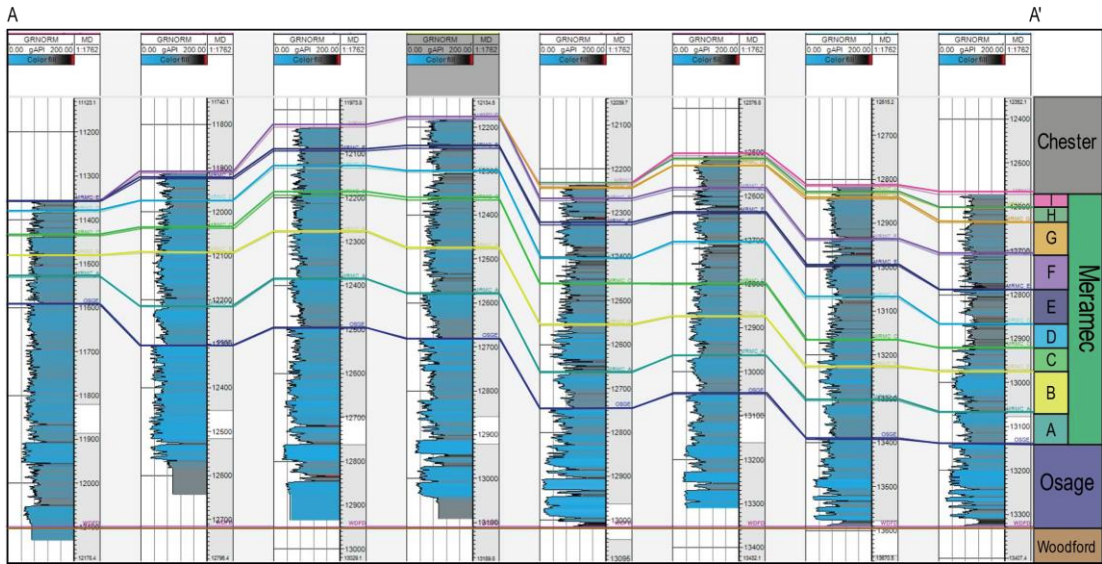
Appendix D-3. Cross-plot of porosity to permeability from core plugs taken from a rock quarry outcrop in northeastern Oklahoma observed in Shelly et al. (2017)
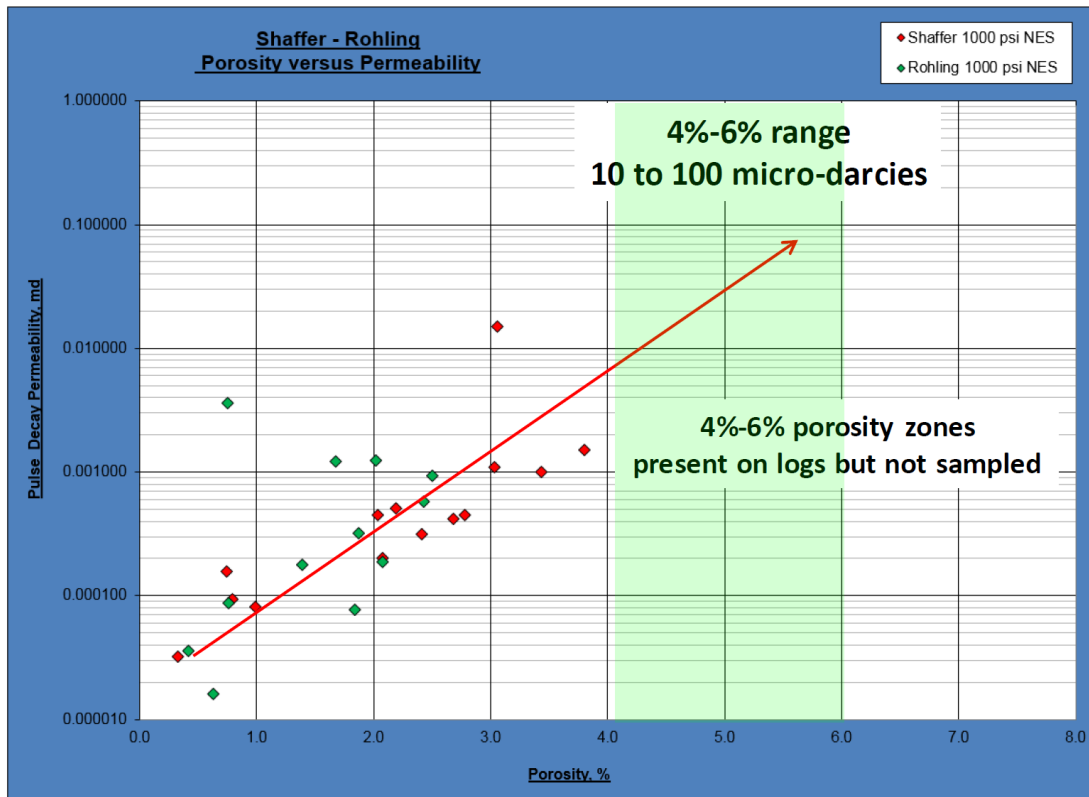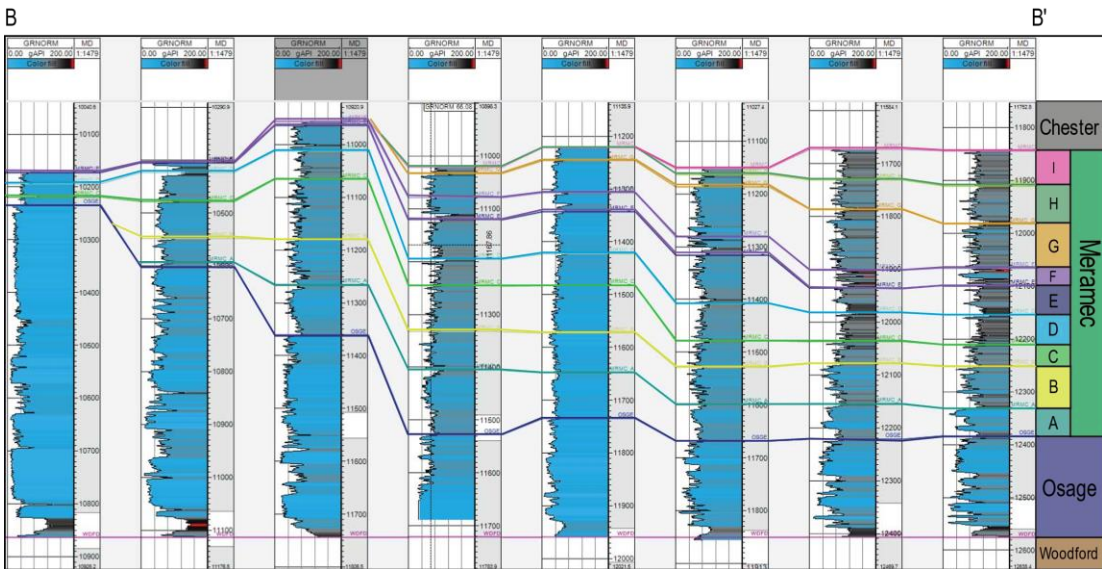
Appendix D-4. Cross plot of porosity and permeability from core samples (Gulf Oil 1-23 Shaffer and Gulf Oil 1-25 Rohling) from Cullen (2017).

Appendix E – Sequence Stratigraphic Architecture

Appendix E-1. Similar sequence stratigraphic framework to the interpretation presented in this study (Price at al., 2017).
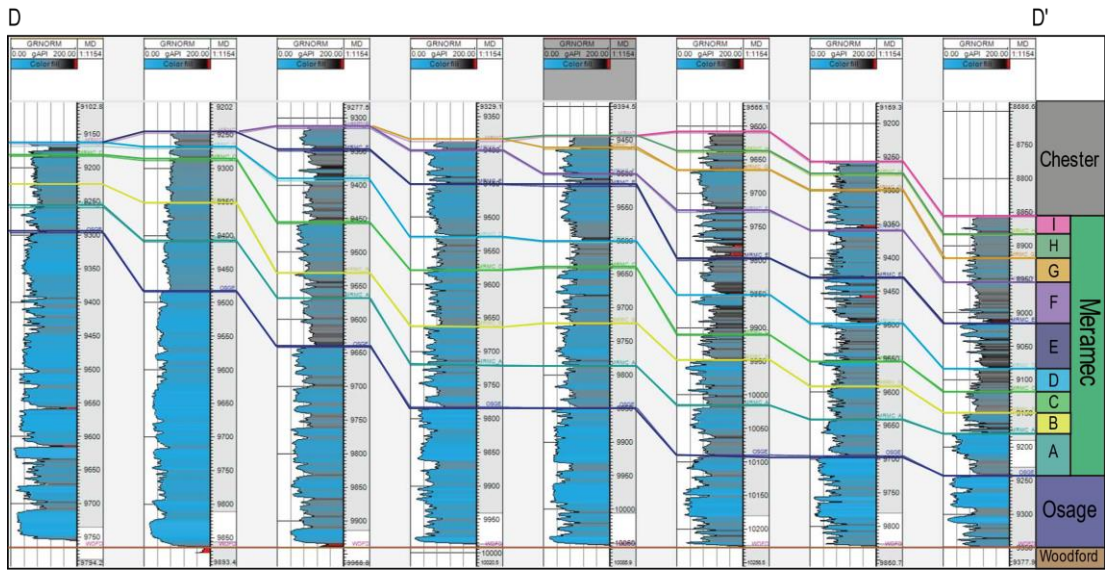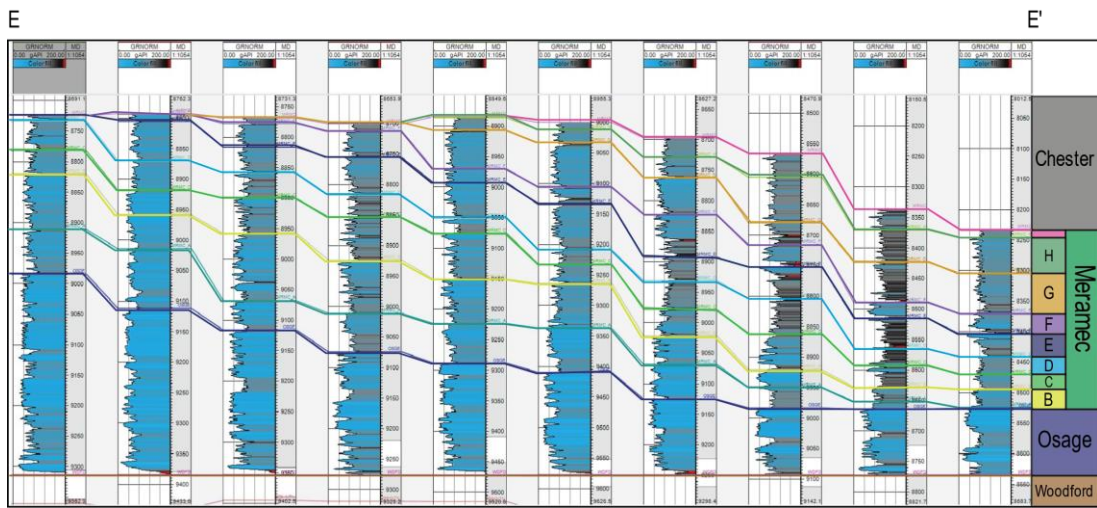
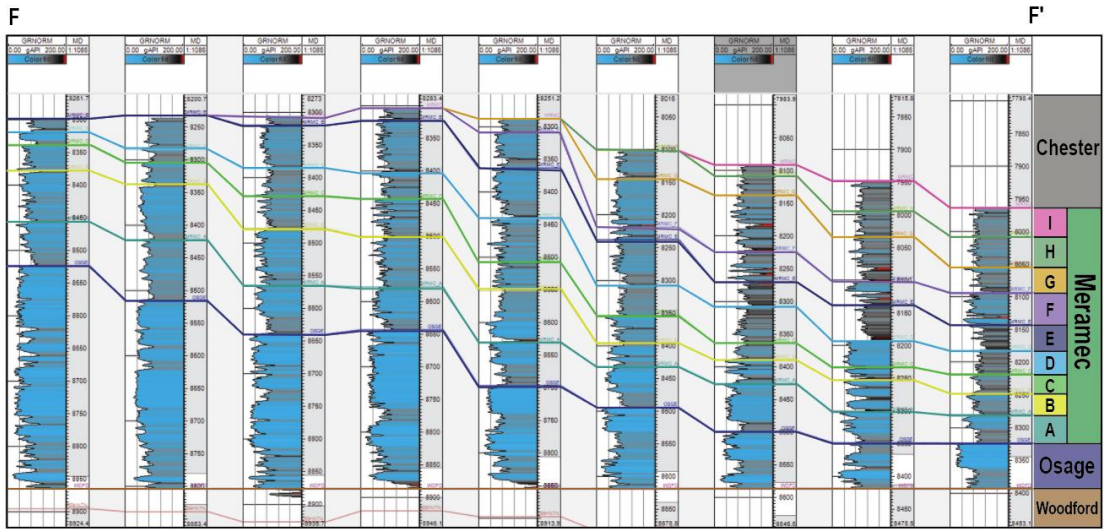Appendix E-2. Cross-section A-A' (Figure 3)

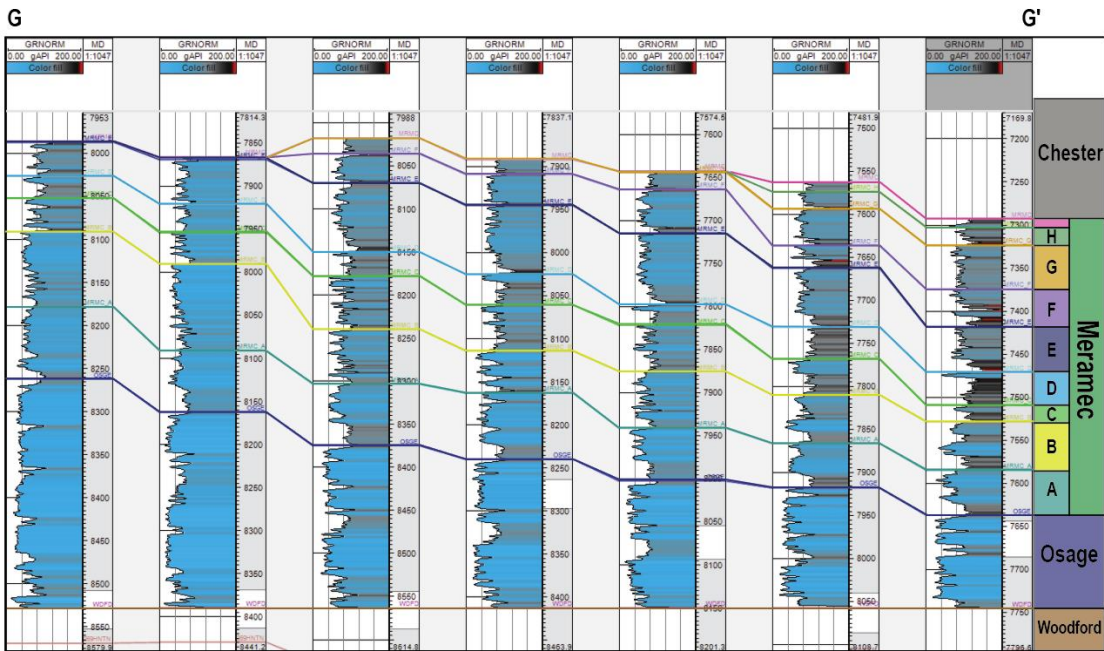Appendix E-3. Cross-section B-B' (Figure 3)
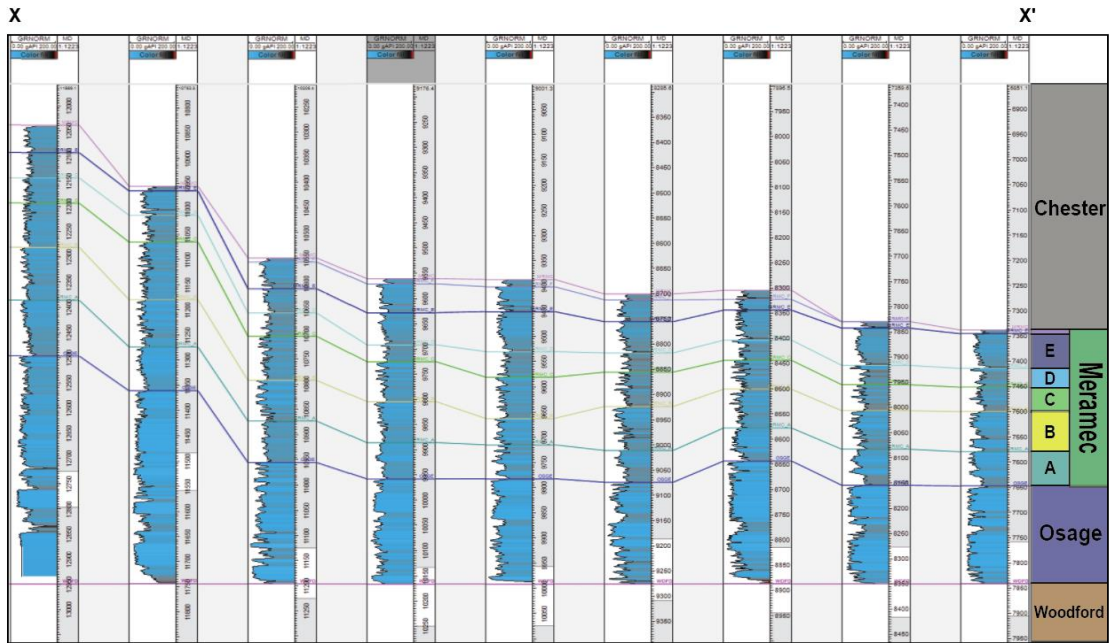
Appendix E-4. Cross-section D-D'

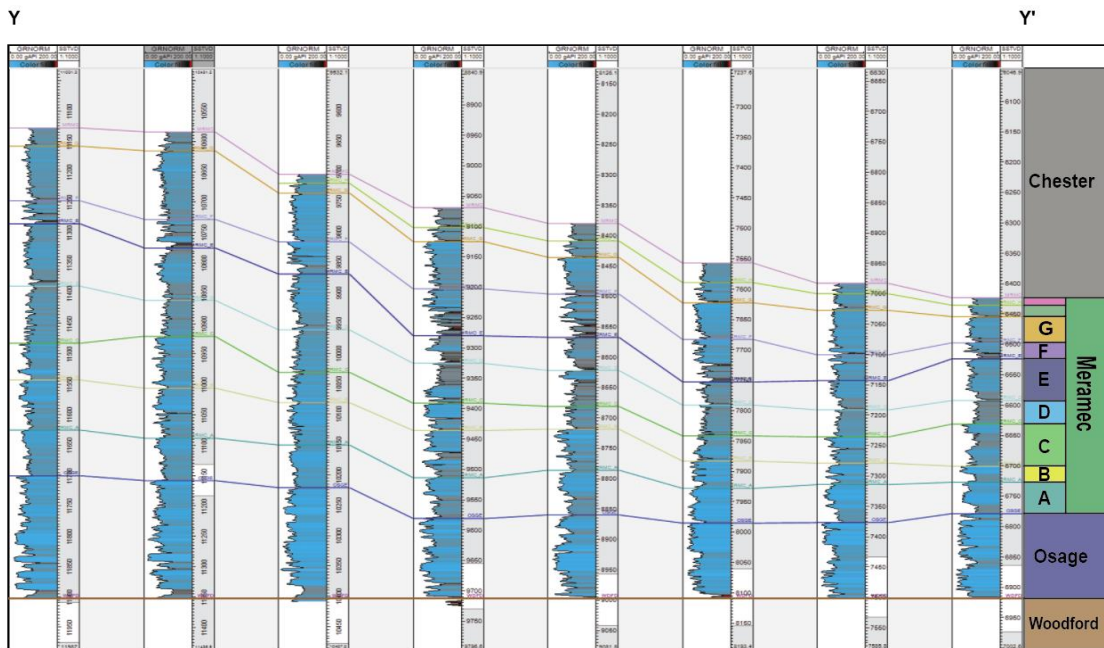Appendix E-5. Cross-section E-E'

Appendix E-6. Cross-section F-F'

Appendix E-7. Cross-section G-G'

Appendix E-8. Cross section X-X' (strike).

Appendix E-9. Cross section Y-Y' (strike).

85

Appendix F – Petrophysical Modeling

Shale Volume Variograms (Calcareous Siltstone)				
Zone	Vertical (ft)	Major (ft)	Minor (ft)	Azimuth (Degrees from N)
MRMC A	8.2	3000	2000	60
MRMC B	7.3	3000	2000	60
MRMC C	7.2	3000	2000	60
MRMC D	5.3	3000	2000	65
MRMC E	7.5	3000	2000	65
MRMC F	8.7	3000	2000	65
MRMC G	8.6	3000	2000	70
MRMC H	6.7	3000	2000	75
MRMC I	3.9	3000	2000	75

Shale Volume Variograms (Highly Calcareous Siltstone)				
Zone	Vertical (ft)	Major (ft)	Minor (ft)	Azimuth (Degrees from N)
MRMC A	6.5	3000	2000	60
MRMC B	6.2	3000	2000	60
MRMC C	5.3	3000	2000	60
MRMC D	9.4	3000	2000	65
MRMC E	7.7	3000	2000	65
MRMC F	5.9	3000	2000	65
MRMC G	8.0	3000	2000	70
MRMC H	6.7	3000	2000	75
MRMC I	5.0	3000	2000	75

Shale Volume Variograms (Argillaceous Calcareous Siltstone)				
Zone	Vertical (ft)	Major (ft)	Minor (ft)	Azimuth (Degrees from N)
MRMC A	6.5	3000	2000	60
MRMC B	6.2	3000	2000	60
MRMC C	5.3	3000	2000	60
MRMC D	9.4	3000	2000	65
MRMC E	7.7	3000	2000	65
MRMC F	5.9	3000	2000	65
MRMC G	8.0	3000	2000	70
MRMC H	6.7	3000	2000	75
MRMC I	5.0	3000	2000	75

Total Porosity Variograms (Calcareous Siltstone)				
Zone	Vertical (ft)	Major (ft)	Minor (ft)	Azimuth (Degrees from N)
MRMC A	8.6	3000	2000	60
MRMC B	7.7	3000	2000	60
MRMC C	9.4	3000	2000	60
MRMC D	5.8	3000	2000	65
MRMC E	5.3	3000	2000	65
MRMC F	5.7	3000	2000	65
MRMC G	5.8	3000	2000	70
MRMC H	7.2	3000	2000	75
MRMC I	7.5	3000	2000	75

Total Porosity Variograms (Highly Calcareous Siltstone)				
Zone	Vertical (ft)	Major (ft)	Minor (ft)	Azimuth (Degrees from N)
MRMC A	8.3	3000	2000	60
MRMC B	7.7	3000	2000	60
MRMC C	7.9	3000	2000	60
MRMC D	7.2	3000	2000	65
MRMC E	7.2	3000	2000	65
MRMC F	6.3	3000	2000	65
MRMC G	5.9	3000	2000	70
MRMC H	7.9	3000	2000	75
MRMC I	7.4	3000	2000	75

Total Porosity Variograms (Argillaceous Calcareous Siltstone)				
Zone	Vertical (ft)	Major (ft)	Minor (ft)	Azimuth (Degrees from N)
MRMC A	8.1	3000	2000	60
MRMC B	8.3	3000	2000	60
MRMC C	8.2	3000	2000	60
MRMC D	6.4	3000	2000	65
MRMC E	6.7	3000	2000	65
MRMC F	6.7	3000	2000	65
MRMC G	5.7	3000	2000	70
MRMC H	7.2	3000	2000	75
MRMC I	7.9	3000	2000	75

Effective Porosity Variograms (Calcareous Siltstone)				
Zone	Vertical (ft)	Major (ft)	Minor (ft)	Azimuth (Degrees from N)
MRMC A	10.9	3000	2000	60
MRMC B	9.1	3000	2000	60
MRMC C	9.8	3000	2000	60
MRMC D	8.6	3000	2000	65
MRMC E	7.0	3000	2000	65
MRMC F	5.1	3000	2000	65
MRMC G	8.7	3000	2000	70
MRMC H	5.5	3000	2000	75
MRMC I	2.4	3000	2000	75

Effective Porosity Variograms (Highly Calcareous Siltstone)				
Zone	Vertical (ft)	Major (ft)	Minor (ft)	Azimuth (Degrees from N)
MRMC A	8.0	3000	2000	60
MRMC B	8.2	3000	2000	60
MRMC C	5.2	3000	2000	60
MRMC D	9.0	3000	2000	65
MRMC E	9.3	3000	2000	65
MRMC F	7.3	3000	2000	65
MRMC G	7.0	3000	2000	70
MRMC H	7.1	3000	2000	75
MRMC I	6.0	3000	2000	75

Effective Porosity Variograms (Argillaceous Calcareous Siltstone)				
Zone	Vertical (ft)	Major (ft)	Minor (ft)	Azimuth (Degrees from N)
MRMC A	9.0	3000	2000	60
MRMC B	10.0	3000	2000	60
MRMC C	8.2	3000	2000	60
MRMC D	7.4	3000	2000	65
MRMC E	6.8	3000	2000	65
MRMC F	8.0	3000	2000	65
MRMC G	8.9	3000	2000	70
MRMC H	5.1	3000	2000	75
MRMC I	6.3	3000	2000	75

Appendix F-1. Variogram parameters for petrophysical models.

| Variogram Parameters for Rock Type Modeling				
Zone	Major (ft)	Minor (ft)	Vertical (ft)	Azimuth (degrees from N)
MRMC A	5000	3500	13	60
MRMC B	5000	3500	16	60
MRMC C	5000	3500	15	60
MRMC D	5000	3500	9	65
MRMC E	5000	3500	9.4	65
MRMC F	5000	3500	9.2	65
MRMC G	5000	3500	10.2	70
MRMC H	5000	3500	10	75
MRMC I	5000	3500	9.8	75

Appendix F-2. Variogram parameters for rock type models.
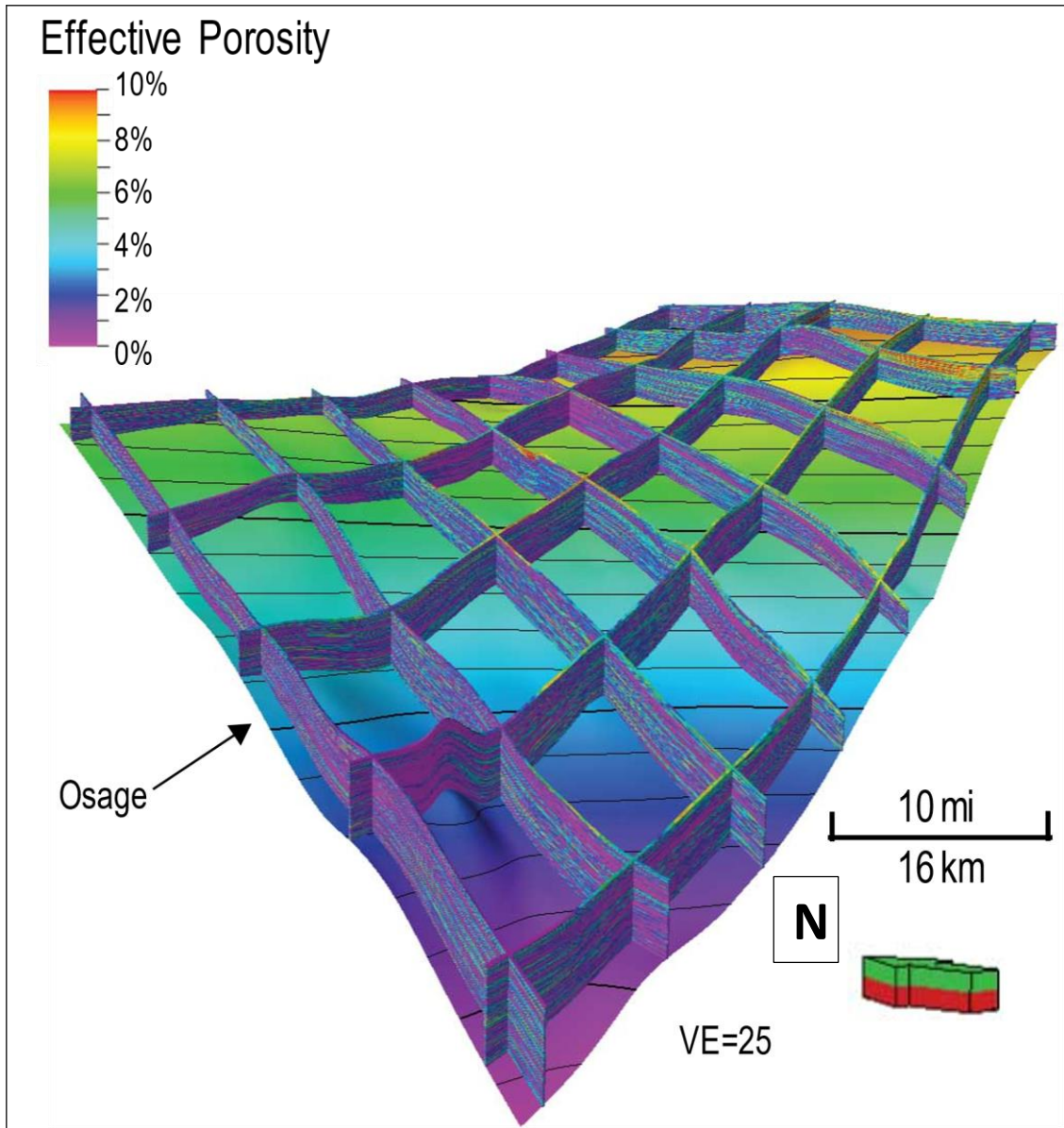
Appendix F-3. Fence diagram through the effective porosity 3-D model. Porosity calculations generally increase basin-ward to the southeast.
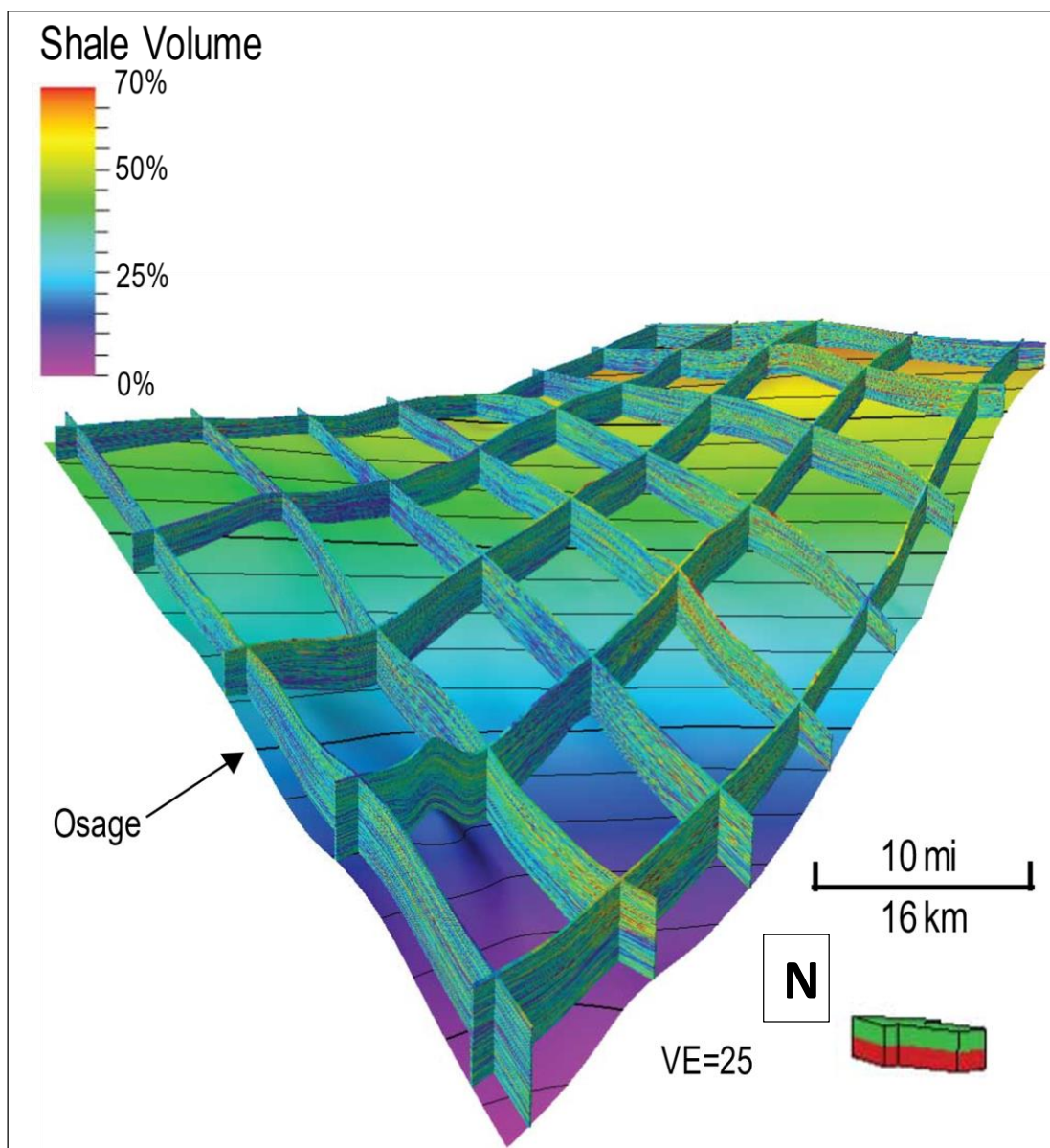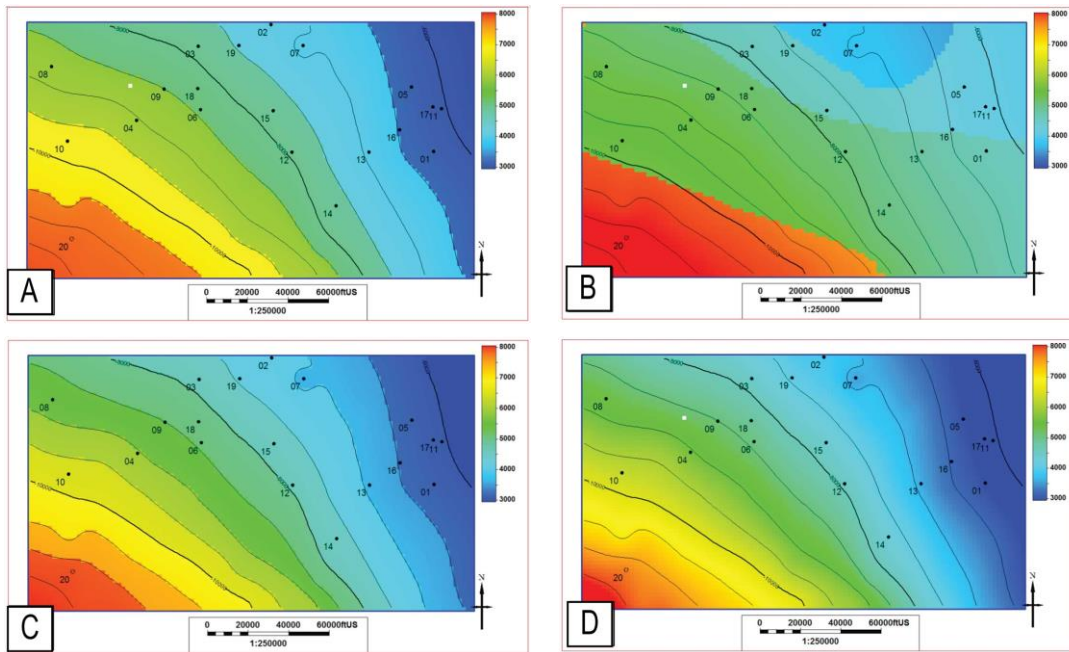
Appendix F-4. Fence diagram of the shale volume 3-D model. Shale volume increases towards the basin in the southeast.
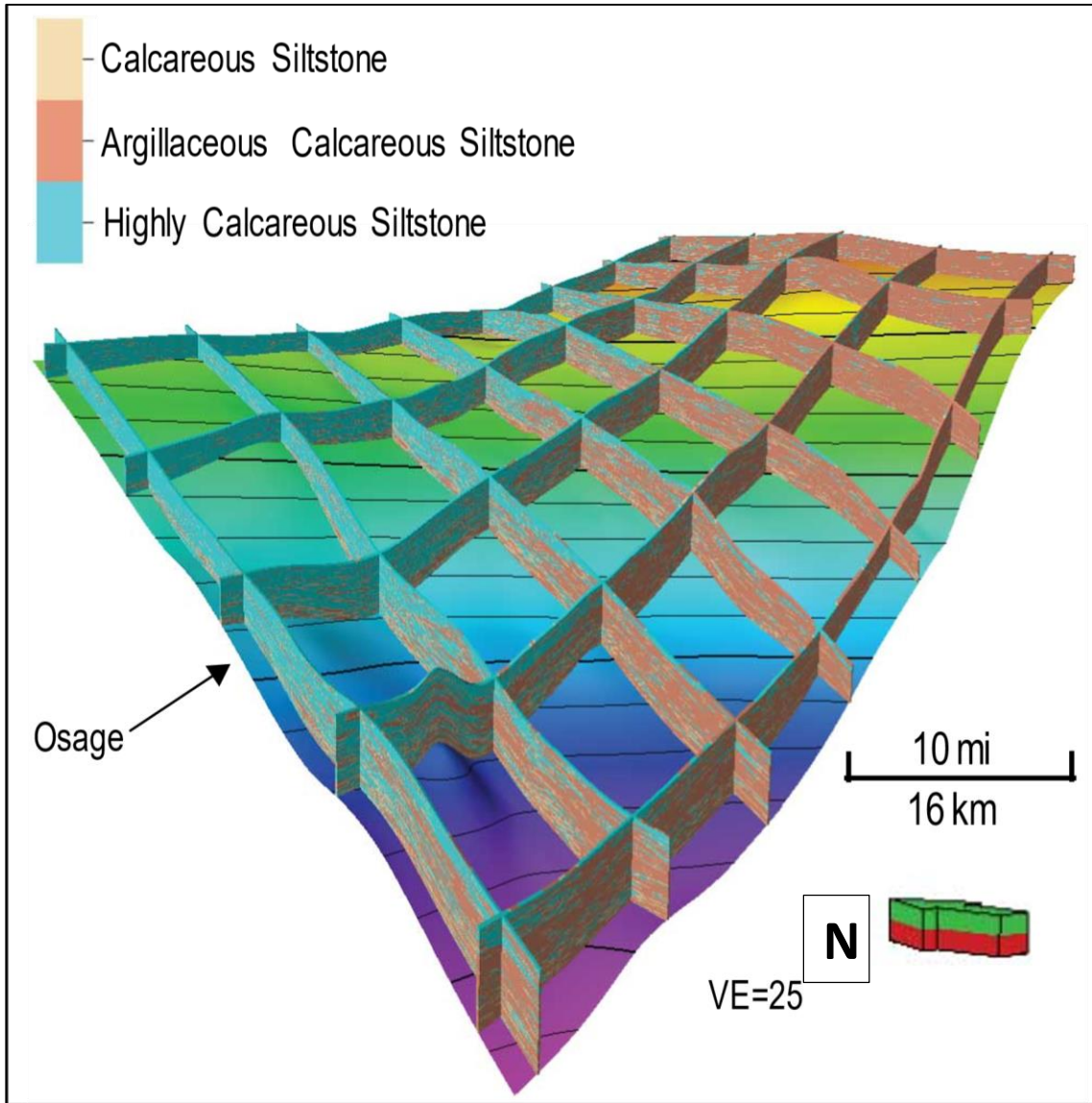
Appendix F-5. Fence diagram of the Lithology 3-D model.

Appendix G – Production Characteristics

Appendix G-1. Reservoir pressure maps indicating the variation in initial reservoir pressure in the Meramec across the study area (Cronk, 2018). These variations are potential drivers for the lack of strong relationships between the lithological and petrophysical properties to well productivity. A-D represent initial reservoir pressure maps constructed using varying reservoir baffle constraints.
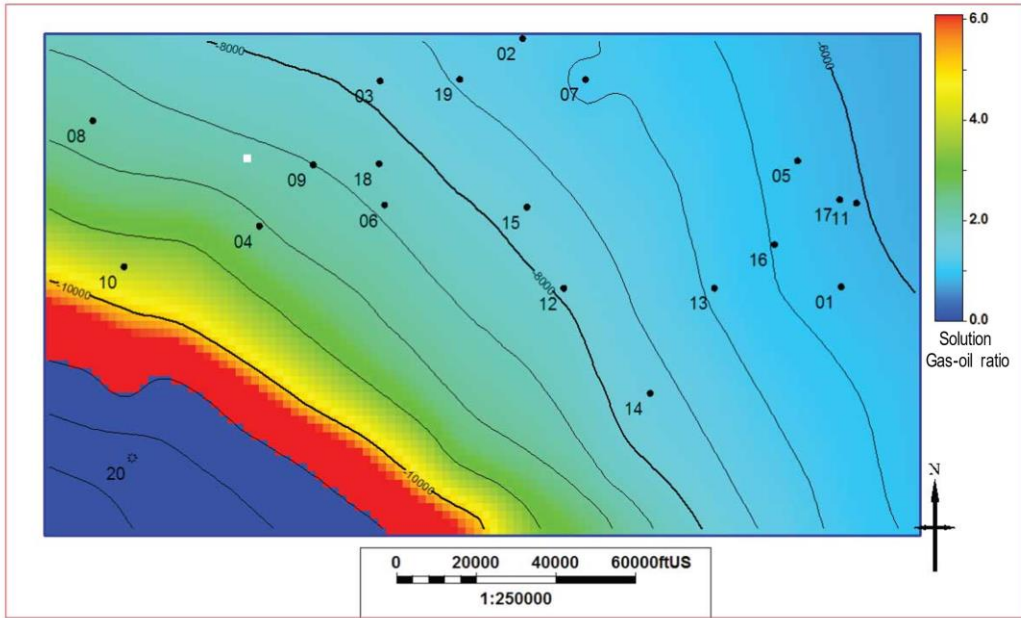
Appendix G-2. Solution gas-oil ratio variations across the study area determined in case-1 of Cronk (2018). Varying fluid properties across the study area likely contribute significantly to production performance of the production wells shown by the black dots.